Article

ILC2-derived LIF licences progress from tissue to systemic immunity

https://doi.org/10.1038/s41586-024-07746-w

Received: 18 September 2023

Accepted: 24 June 2024

Published online: 7 August 2024

Open access

Check for updates

Mayuri Gogoi[1]✉, Paula A. Clark[1], Ana C. F. Ferreira[1,2], Noe Rodriguez Rodriguez[1,2], Morgan Heycock[1], Michelle Ko[1], Jane E. Murphy[1], Victor Chen[1], Shi-Lu Luan[1], Helen E. Jolin[1,2] & Andrew N. J. McKenzie[1]✉

Migration and homing of immune cells are critical for immune surveillance. Trafficking is mediated by combinations of adhesion and chemokine receptors that guide immune cells, in response to chemokine signals, to specific locations within tissues and the lymphatic system to support tissue-localized immune reactions and systemic immunity[1,2]. Here we show that disruption of leukaemia inhibitory factor (LIF) production from group 2 innate lymphoid cells (ILC2s) prevents immune cells leaving the lungs to migrate to the lymph nodes (LNs). In the absence of LIF, viral infection leads to plasmacytoid dendritic cells (pDCs) becoming retained in the lungs where they improve tissue-localized, antiviral immunity, whereas chronic pulmonary allergen challenge leads to marked immune cell accumulation and the formation of tertiary lymphoid structures in the lung. In both cases immune cells fail to migrate to the lymphatics, leading to highly compromised LN reactions. Mechanistically, ILC2-derived LIF induces the production of the chemokine CCL21 from lymphatic endothelial cells lining the pulmonary lymphatic vessels, thus licensing the homing of $CCR7^+$ immune cells (including dendritic cells) to LNs. Consequently, ILC2-derived LIF dictates the egress of immune cells from the lungs to regulate tissue-localized versus systemic immunity and the balance between allergen and viral responsiveness in the lungs.

The lungs are constantly exposed to the inhalation of both infectious and non-infectious agents. The immune system must respond efficiently and appropriately to combat respiratory pathogens and/or repair tissue damage but also avoid inappropriate and potentially harmful inflammation such as allergic asthma[3] or virus-induced pathology[4]. The emplacement of innate lymphoid cells (ILCs) as immune sentinels within mucosal surfaces allows them to survey tissues to help counter inappropriate immune reactions and maintain homeostasis, but also to react rapidly to protect against infection or injury[5–7]. This requires the orchestration of a highly dynamic system in which the circulation and homing of specialized immune cells must be coordinated in response to tissue-derived cues[3,5].

During allergen-induced chronic type 2 lung inflammation, alarmin-like cytokines such as interleukin-33 (IL-33), IL-25 and thymic stromal lymphopoietin activate ILC2 proliferation and the vigorous production of type 2 effector cytokines (including IL-4, IL-5, IL-13 and amphiregulin) promoting T helper 2 (T_H2) cell differentiation, immunoglobulin E (IgE) production, eosinophilia, mucus hypersecretion and airway contraction, but also aberrant tissue repair that can lead to fibrosis[3]. Lung ILC2s also have roles in the regulation of type 1 responses to infection by respiratory viruses including rhinovirus[8], influenza virus[9,10] and respiratory syncytial virus (RSV)[11], with dysregulation associated experimentally with viral-induced asthma exacerbation[12]. Similarly, imbalanced pathogen-induced inflammation, as opposed to tissue repair, can lead to immune-mediated pathology. For example, infection with influenza A virus or severe acute respiratory syndrome coronavirus 2 (SARS-CoV-2) induces type I interferon production from pDCs, which may act antivirally or contribute to immunopathology[13,14].

Cell migration and homing help control the differential magnitude of localized pulmonary tissue responses versus the dissemination of systemic immune responses following allergen or virus exposure[15–19]. Indeed, following the disruption of the CCL21 chemokine–CCR7 chemokine receptor pathway, rather than DCs and antigen-specific T cells and B cells migrating to the secondary lymphoid organs (lymph nodes, LNs) to expand before returning to the inflamed tissues, they remain in the lung to develop tertiary lymphoid structures (TLS) in the form of inducible bronchus-associated lymphoid tissues (iBALT). This tissue-localized inflammation can lead to enhanced antiviral immunity[19] but is also associated with chronic allergic responses[15–18,20]. Here we investigated how ILC2s can modify the lung microenvironment to promote systemic immunity and counterbalance tissue-localized antiviral responses.

ILC2s are required for normal homing of pDCs

Using multiparametric flow cytometry to characterize rapid immune cell changes in the lung during the onset of a type 2 immune response

[1]MRC Laboratory of Molecular Biology, Cambridge, UK. [2]These authors contributed equally: Ana C. F. Ferreira, Noe Rodriguez Rodriguez, Helen E. Jolin. ✉e-mail: mgogoi@mrc-lmb.cam.ac.uk; anm@mrc-lmb.cam.ac.uk

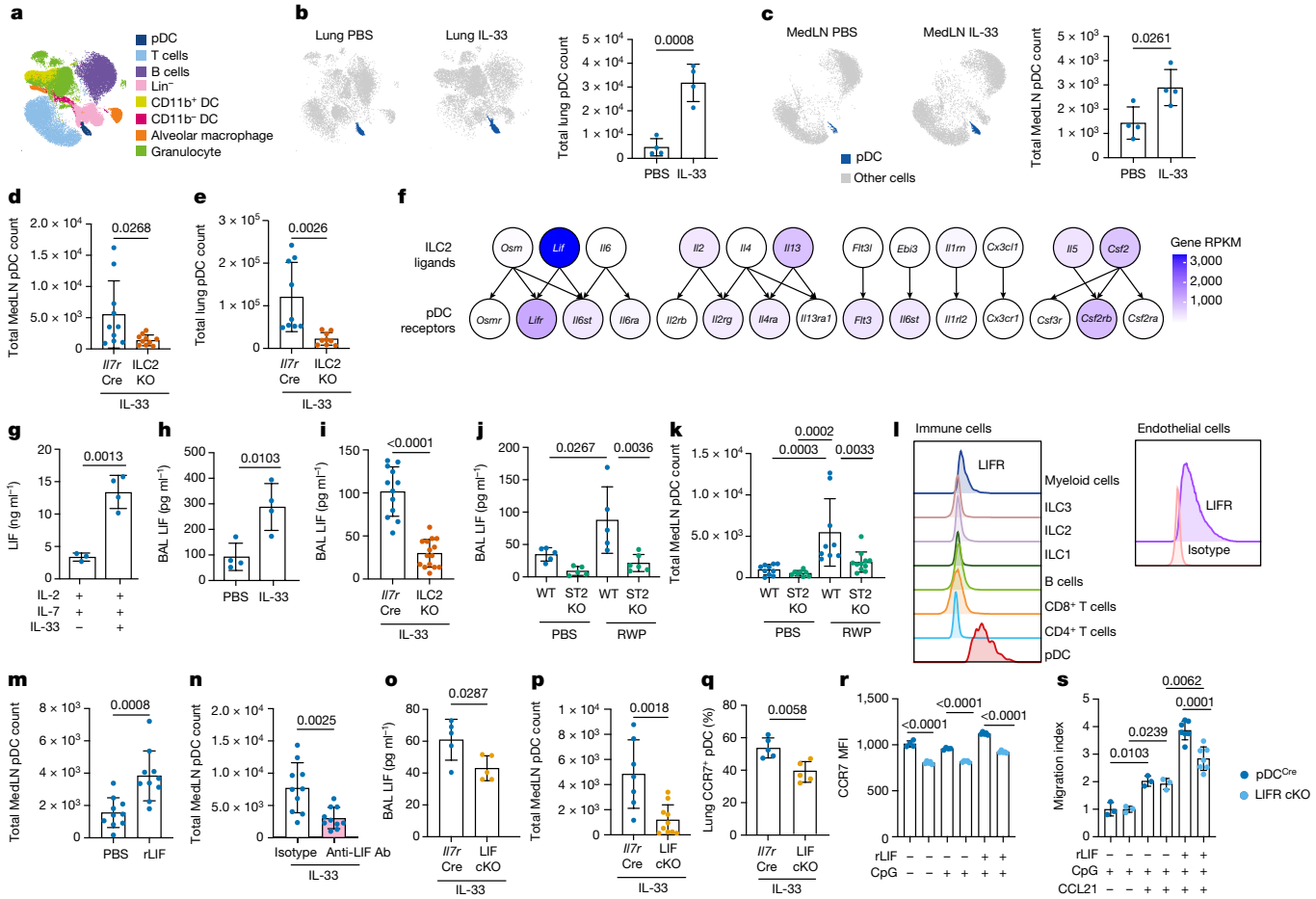

Fig. 1 | ILC2s are required for normal homing of pDCs. a–**c**, Uniform manifold approximation and projection of lung and MedLN immune cell clusters (**a**) and quantification of pDCs (**b**,**c**) from flow cytometry analysis following PBS and IL-33 intranasal treatment of lung (**b**) and MedLN (**c**) in WT mice ($n = 4$). **d**,**e**, Flow cytometry analysis of *Il7r*^{Cre} and *Il7r*^{Cre}*Rora*$^{flox/flox}$ pDCs in MedLN (**d**, $n = 10$) and lung (**e**, $n = 9$). **f**, Heatmap of ligand and receptor expression derived from RNA-seq data. **g**–**j**, ELISA of LIF from purified ILC2s cultured with IL-2 + IL-7, with ($n = 4$) or without ($n = 3$) IL-33 (**g**); BAL of mice treated with IL-33 (**h**, WT, $n = 4$; **i**, *Il7r*^{Cre}, $n = 12$; ILC2KO, $n = 15$); and with either ragweed protein (RWP, **j**, WT, $n = 5$; ST2KO, $n = 6$) or PBS (WT, $n = 5$; ST2KO, $n = 5$). **k**, Flow cytometry analysis of pDCs (WT: PBS, $n = 10$; RWP, $n = 9$; ST2KO: PBS, $n = 8$; RWP, $n = 11$). **l**, Flow cytometry analysis of LIF receptor (LIFR) on indicated cell types. **m**,**n**, Flow cytometry analysis of pDCs in WT mice following rLIF treatment (**m**, $n = 10$) and anti-LIF neutralizing antibody (Ab) and IL-33 treatment (**n**, $n = 10$). **o**, ELISA of BAL LIF following IL-33 challenge ($n = 5$). **p**,**q**, Flow cytometry analysis of pDCs in *Il7r*^{Cre} ($n = 7$) and LIF-cKO ($n = 10$) (**p**), and lung CCR7$^+$ pDC (**q**) percentage ($n = 5$), following IL-33 challenge. **r**, Flow cytometry analysis of CCR7 expression by CpG-activated pDC^{Cre} and LIFR-cKO pDCs with or without rLIF for 16 h (pDC^{Cre}, $n = 4$; pDC^{Cre} + CpG, $n = 4$; pDC^{Cre} + CpG + rLIF, $n = 5$; LIFR-cKO, $n = 5$; LIFR-cKO + CpG, $n = 5$; LIFR-cKO + CpG + rLIF, $n = 5$). **s**, Chemotaxis of CpG-activated pDC^{Cre} or LIFR-cKO pDCs to CCL21 with or without rLIF for 16 h (pDC^{Cre} + CpG, $n = 3$; pDC^{Cre} + CpG + CCL21, $n = 3$; pDC^{Cre} + CpG + rmLIF + CCL21, $n = 7$; LIFR-cKO + CpG, $n = 3$; LIFR-cKO + CpG + CCL21, $n = 3$; LIFR-cKO + CpG + rmLIF + CCL21, $n = 7$). **b**–**e**,**g**–**i**,**m**–**s**, Unpaired two-sided *t*-test; **j**,**k**, one-way analysis of variance (ANOVA) with Tukey's multiple-comparisons test; data (mean ± s.e.m.) are either representative (**a**–**c**,**g**,**h**,**j**,**l**,**o**,**q**–**s**) or pooled from two independent experiments (**d**,**e**,**i**,**k**,**m**,**n**,**p**). Lineage (Lin) contains CD3, CD4, CD8a, CD19, CD11b, CD11c and FcER1 antibodies; RPKM, reads per kilobase per million mapped reads.

induced by acute treatment with recombinant mouse IL-33 (refs. 21,22), we noted an unexpected increase in CD45$^+$CD317$^+$Siglec-H$^+$F4/80$^-$CD11b$^-$ pDCs in the lung and the lung-draining mediastinal LN (MedLN) (Fig. 1a–c). pDCs develop in the bone marrow and are key producers of antiviral type I IFN, which drives innate antiviral responses[23]. During inflammation, pDCs upregulate chemokine receptors and are rapidly recruited from the circulation into the spleen and peripheral LNs (CCR7-, CXCR3- and CCR5-mediated)[23] or intestinal tissue (CCR9-mediated)[24]. Although gene expression analysis confirmed the phenotype of lung pDCs (Extended Data Fig. 1a), these did not express the IL-33 receptor (ST2, *Il1rl1* gene; Extended Data Fig. 1a,b), suggesting an indirect mechanism by which IL-33 induces pDCs. By treating T cell- and B cell-deficient (*Rag2*$^{-/-}$) mice or lymphocyte-deficient (*Rag2*$^{-/-}$*Il2rg*$^{-/-}$) mice with IL-33, we determined that ILCs are required for the IL-33-induced pDC increase but that T cells and B cells are not (Extended Data Fig. 1c,d). IL-33-treated, ILC2-deficient (ILC2KO, *Il7r*^{Cre}*Rora*$^{flox/flox}$) mice also failed to induce pDCs, indicating a role for ILC2s in pDC regulation (Fig. 1d,e).

ILC2-derived LIF regulates pDC migration to LNs

For identification of potential ILC2-derived regulators of pDC biology we cross-referenced cytokine receptors expressed by pDCs with cytokine ligands produced by ILC2s. LIF, produced by ILC2s, and LIF receptor (LIFR), expressed by pDCs, represented attractive targets (Fig. 1f) because the role of ILC2-derived LIF is unknown and LIF can negatively regulate pDC development and type I IFN production[25,26]. LIF is a pleiotropic cytokine with roles in embryonic development and promotion of tumorigenesis, but its functions in immunity are understudied[27]. *Lif* was expressed by ILC2s from several tissues (Extended Data Fig. 1e), and LIF protein was produced by in vitro cultured ILC2s (Fig. 1g) and in vivo in bronchoalveolar lavage (BAL) in response to IL-33

(Fig. 1h), independently of T lymphocytes and B lymphocytes (Extended Data Fig. 1f) but requiring ILC2s (Fig. 1i). Short-term administration of ragweed pollen (RWP) extract, an inducer of ILC2-dependent allergic immune reactions in the lung[21], also upregulated LIF production (Extended Data Fig. 1g), which required ILC2s (Extended Data Fig. 1h) and signalling via the ST2 receptor (assessed using ST2-deficient mice) correlating with fewer pDCs in the MedLN (Fig. 1j,k and Extended Data Fig. 1i).

Next we determined the expression of LIFR on lung cells. Little LIFR was observed on ILC1s, ILC2s, ILC3s, T cells, B cells or myeloid cells (Fig. 1l and Extended Data Fig. 1j) but was present on pDCs and $CD31^+$ endothelial cells (Fig. 1l). Bone marrow-derived pDCs also responded to ILC2-derived LIF as determined by their phosphorylation of STAT3 (p-STAT3), a key signalling component of the LIFR signalling pathway[25,26], which was ablated by the inclusion of anti-LIF neutralizing antibody (Extended Data Fig. 1k). Furthermore, intranasal administration of recombinant LIF (rLIF) induced pDCs in both MedLN and lung (Fig. 1m and Extended Data Fig. 1l) whereas anti-LIF neutralizing antibody inhibited pDC induction following IL-33 treatment in vivo (Fig. 1n and Extended Data Fig. 1m). The increase in pDCs occurred within 6 h (Extended Data Fig. 1n) in the absence of changes in pDC proliferation (Extended Data Fig. 1o), suggesting that pDC accumulation had resulted from recruitment rather than cell division. However, LIF did not induce pDC migration directly (Extended Data Fig. 1p).

For investigatation of the roles of ILC2-derived LIF we generated $Il7r^{Cre}Lif^{flox/flox}$ (LIF-cKO) mice to delete LIF in lymphocytes (Extended Data Fig. 1q–t). Intranasal administration of IL-33 to LIF-cKO mice resulted in reduced LIF concentrations in BAL (Fig. 1o) and fewer pDCs in the MedLN (Fig. 1p). However, lung pDCs were not reduced (Extended Data Fig. 1u), in contrast to the reduction observed in ILC2-deficient mice, suggesting that additional ILC2-dependent factors may also be in play. Similar results were obtained from RWP challenge of LIF-cKO mice (Extended Data Fig. 1v). Interestingly, although lymphocyte-derived LIF did not account for all LIF detected in the BAL, other sources of LIF were not capable of rescuing the observed phenotype. This suggests a more localized action for lymphocyte-derived LIF, such as in stromal cell niches within lung perivascular adventitial cuffs in which tissue-resident ILC2s are known to be present[28]. For assessment of the role of ILC2-derived LIF, we transferred either purified LIF-producing ILC2s or LIF-deficient ILC2s into ILC2KO mice and then challenged them with RWP. Transfer of LIF-producing ILC2s resulted in more pDCs in MedLNs than induced by LIF-deficient ILC2s (Extended Data Fig. 1w). There was no difference in lung pDC numbers (Extended Data Fig. 1x). Thus, ILC2-derived LIF is sufficient to enhance pDC numbers in MedLNs. For visualization of the defect in the migration of pDCs from the lung to MedLN we delivered fluorescein isothiocyanate (FITC)-dextran intranasally into the lungs of mice and assessed the migration of FITC-labelled pDCs to the MedLN in response to IL-33 lung challenge (Extended Data Fig. 1y). LIF-cKO mice showed reduced migration of FITC-dextran-positive pDCs from the lung to the MedLN as compared with controls (Extended Data Fig. 1z), demonstrating LIF-mediated regulation of pDC migration.

We also investigated the reciprocal part played by LIFR expression on pDCs by intercrossing pDC^{Cre} ($Tg^{Siglech\text{-}Cre,\text{-}mCherry}$) mice with $Lifr^{-/flox}$ mice (Extended Data Fig. 2a). Despite inefficient LIFR deletion from pDCs (Methods and Extended Data Fig. 2b), $pDC^{Cre}Lifr^{-/flox}$ mice showed impaired pDC induction in MedLNs (but not in lungs) following RWP challenge as compared with controls (Extended Data Fig. 2c,d), mirroring mice lacking LIF production from lymphocytes. Bone marrow-derived pDCs from $pDC^{Cre}Lifr^{-/flox}$ mice also showed reduced STAT3 phosphorylation as compared with control (Extended Data Fig. 2e). Thus ILC2-derived LIF is produced in response to IL-33 and allergen challenge and regulates the proportions of pDCs in both lung tissue and MedLN.

LIF promotes CCR7 expression on pDCs

For identification of cell migration-related factors induced in pDC by IL-33, we re-examined the RNA sequencing (RNA-seq) data from pDCs purified from the lungs of wild-type (WT) mice challenged intranasally with PBS or IL-33 (Extended Data Fig. 2f). The 'cytokine–cytokine receptor interaction and chemokine signalling' pathway was identified as the top hit from Kyoto Encyclopedia of Genes and Genomes (KEGG) pathway analysis of all genes with significant differential expression (Extended Data Fig. 2g). Notably, the chemokine receptor CCR7 was upregulated by IL-33 treatment (Extended Data Fig. 2h). CCR7 is important for lymphocyte migration into LNs[29] and is also upregulated on pDCs following activation; CCR7-deficient pDCs show markedly impaired homing to LNs[30]. We found fewer $CCR7^+$ pDCs in the lungs of LIF-cKO mice challenged intranasally with either IL-33 or RWP (Fig. 1q and Extended Data Fig. 2i,j). Notably, bone marrow-derived pDCs (which in our cultures were $CCR7^+$ before CpG activation) showed that LIFR-deficient pDCs expressed less CCR7 (Fig. 1r) and evidenced reduced migration towards CCL21 (a CCR7 ligand) in the presence of rLIF compared with controls (Fig. 1s), although this may have been underestimated due to inefficient LIFR deletion from pDCs (Methods and Extended Data Fig. 2b). These data support a role for LIF-induced CCR7 expression on pDCs in their recruitment to MedLN.

LIF promotes virus-induced $CCR7^+$ cell migration

Given the importance of pDCs in immune responses to viruses, we next used pneumovirus of mice (PVM), a natural pathogen of mice that replicates in the respiratory tract (Extended Data Fig. 2k) and that can be used to model many of the pathological features of human RSV infection, including potent type I IFN production[31,32]. Eight days after PVM infection, increased LIF was detected in the BAL of control mice compared with LIF-cKO mice (Extended Data Fig. 2l), with lung ILC2s representing the predominant source of *Lif* as compared with T cells (Extended Data Fig. 2m). Notably, the lungs of PVM-infected LIF-cKO mice showed more virus-induced inflammatory cell aggregates (Fig. 2a and Extended Data Fig. 2n), which was accompanied by improved antiviral immunity as indicated by a reduced viral load (Fig. 2b). There was little increase in lung pDCs in LIF-cKO mice (Extended Data Fig. 2o and see below); however, there was an elevation in type I IFN in BAL (Extended Data Fig. 2p) suggesting that, by deletion of LIF, pDCs were no longer being inhibited thus resulting in greater type I IFN production and a reduction in IL-5 (Fig. 2c and Extended Data Fig. 2p–r), aligning with the potential of type I IFN to inhibit ILC2s[9,10]. However, lung eosinophils, neutrophils, alveolar macrophages and monocytes were unchanged (Extended Data Fig. 2s). By stark contrast, lung-draining MedLNs were notably smaller in the absence of LIF following viral challenge (Fig. 2d), which was associated with a profound deficit in all $CD45^+$ immune cells in the MedLN but not in the lung (Fig. 2e and Extended Data Fig. 2t). This included T cells, B cells, conventional dendritic cells (cDCs) and pDCs as compared with controls (Extended Data Fig. 2u–x). Similar to the results observed in IL-33 and RWP challenge, PVM infection also resulted in a smaller proportion of pDCs expressing CCR7 (but not other chemokine receptors) in the absence of LIF (Extended Data Fig. 2y,z). For visualization and corroboration of the defect in cell migration, we labelled lung immune cells with FITC-dextran and assessed their homing to MedLN following lung challenge with PVM (Extended Data Fig. 3a). LIF-cKO mice showed reduced migration of FITC-labelled immune cells (predominantly DCs) to the MedLN compared with controls (Extended Data Fig. 3b–d). Furthermore, by intravenous administration of anti-CD45-APC antibody to label circulating blood cells during PVM infection, we confirmed that the LIF-dependent immune cell deficit in the MedLN had resulted from their impaired migration from the lungs via the lymphatic system, although the magnitude of the immune response

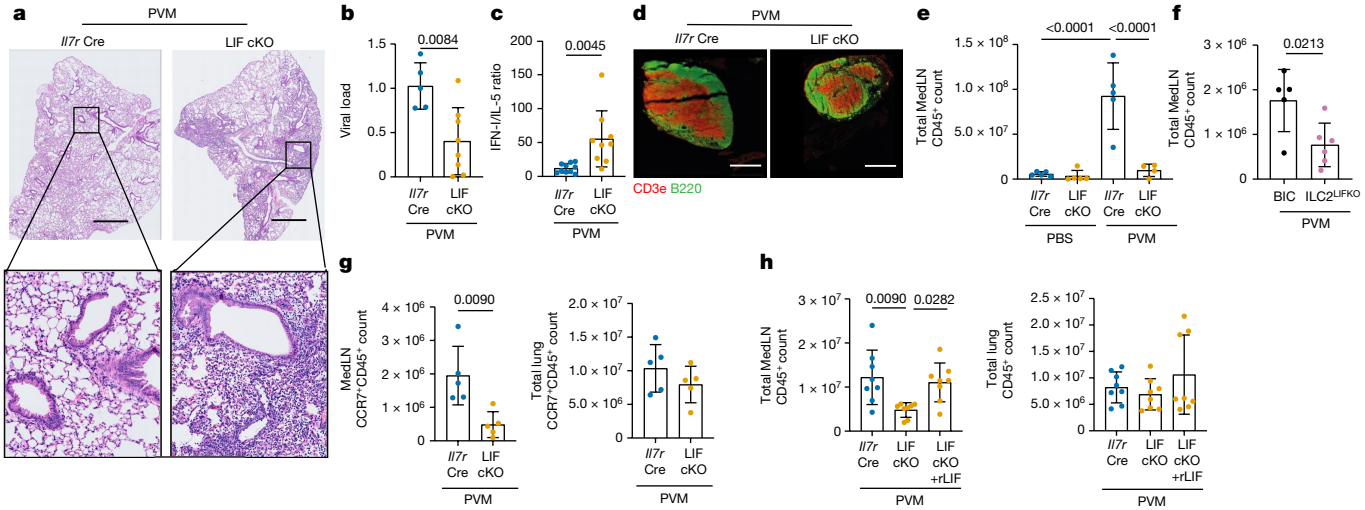

Fig. 2 | ILC2-derived LIF is required for all CCR7$^+$ immune cell egress to LNs. **a**, Lung histology from *Il7r*^{Cre} and LIF-cKO mice following PVM challenge at day 8. **b**, Lung viral load following PVM challenge in *Il7r*^{Cre} ($n = 5$) and LIF-cKO ($n = 8$) mice. **c**, BAL type I IFN (IFN-I):IL-5 ratio from ELISA data following PVM challenge by *Il7r*^{Cre} ($n = 10$) and LIF-cKO ($n = 9$) mice. **d**, Histology of *Il7r*^{Cre} and LIF-cKO mouse MedLN following PVM challenge. B cells were stained with B220 antibody (green), T cells with CD3e antibody (red). **e**,**f**, Flow cytometry analysis of CD45$^+$ cell numbers following PVM challenge in *Il7r*^{Cre} (PBS, $n = 5$; PVM, $n = 5$) and LIF-cKO (PBS, $n = 5$; PVM, $n = 4$) mice (**e**) and in BIC ($n = 5$) and BIC × *Lif*$^{flox/flox}$ (ILC2^{LIFKO}, $n = 6$) mice (**f**). **g**, Flow cytometry analysis of CCR7$^+$CD45$^+$ cell numbers following PVM challenge in *Il7r*^{Cre} and LIF-cKO mice ($n = 5$). **h**, CD45$^+$ cell numbers in *Il7r*^{Cre} and LIF-cKO mice treated with rLIF and infected with PVM (*Il7r*^{Cre} + PVM, $n = 8$; LIF-cKO + PVM, $n = 8$; LIF-cKO + PVM + rLIF, $n = 8$). **b**,**c**,**f**,**g** Unpaired two-sided *t*-test; **e**,**h**, one-way ANOVA with Tukey's multiple-comparisons test. Data presented as mean ± s.e.m. **a**,**d**–**g**, Data are representative of two independent experiments with similar results. **b**,**c**,**h**, Experiments are pooled data from two independent experiments. Scale bars, 1,000 µm (**a**), 200 µm (**d**).

to infection was smaller in these experiments, leading to more modest differences between LIF-cKO mice and controls (Extended Data Fig. 3e–j).

To confirm the specific requirement for ILC2-derived LIF in CD45$^+$ immune cell homing in response to PVM, we used Boolean-ILC2-Cre (BIC)-targeting mice[33] intercrossed with *Lif*$^{flox/flox}$ mice to produce ILC2^{LIFKO} mice (Extended Data Fig. 3k). Quantitative PCR (qPCR) confirmed the deletion of *Lif* in ILC2s, but not in T cells or B cells (Extended Data Fig. 3l). Following PVM infection of ILC2^{LIFKO} mice we again observed improved antiviral immunity, as indicated by reduced viral load (Extended Data Fig. 3m). Although lung eosinophils, neutrophils, alveolar macrophages and monocytes were unchanged (Extended Data Fig. 3n), there was a substantial impairment of CD45$^+$ immune cell numbers in the MedLN (including T cells, B cells, pDCs and cDCs) but not in the lung (Fig. 2d and Extended Data Fig. 3o–s). This corresponded with reduced numbers of CCR7$^+$CD45$^+$ immune cells (Fig. 2g and Extended Data Fig. 4a–c), suggesting that the CCL21–CCR7 cell homing signal may be dysregulated across all these immune cell subsets in the absence of LIF. However, unlike LIFR$^+$ pDCs which we showed can respond directly to LIF by upregulation of CCR7 expression, we did not observe changes in the proportions of other lung immune cells expressing CCR7 in the presence or absence of LIF signalling (Extended Data Fig. 4d). Nevertheless, the immune cell homing defect could be reversed by injection of PVM-infected LIF-cKO mice with rLIF (Fig. 2h and Extended Data Fig. 4e,f), indicating that the immune cell deficit is LIF dependent. These results raised the possibility that, rather than regulating only CCR7 expression on pDCs, LIF also controls the expression of CCR7 ligands, CCL21 and/or CCL19 to modulate all CCR7$^+$CD45$^+$ immune cell homing. These data suggest the existence of a previously unappreciated role for ILC2-derived LIF in regulation of immune cell egress from lung to MedLN.

LIF induces CCL21 from lymphatic endothelial cells

For investigation of this LIF-regulated immune cell homing pathway, we first assessed whether immune cells were failing to be retained in the MedLN. LIF-cKO or control mice were infected with PVM and treated with either sphingosine 1-phosphate analogue FTY720 (which blocks lymphocyte egress from LNs[34]) or PBS (Extended Data Fig. 5a). No accumulation of lymphocytes was observed in either the LNs or lung of FTY720-treated LIF-cKO mice (Extended Data Fig. 5b–g), in contrast to PBS-treated controls, whereas there were comparable numbers of CD45$^+$ immune cells in the spleen and thymus (Extended Data Fig. 5h,i), supporting the proposal that T cells, B cells and DCs were not reaching the LN in the absence of LIF.

We next re-examined the identity of the endothelial LIFR$^+$ cells that we had observed in the lung and identified them as CD45$^-$CD31$^+$podoplanin$^+$ lymphatic endothelial cells (LECs), which comprise the wall of pulmonary lymphatic vessels, and blood vascular endothelial cells (BECs, CD45$^-$CD31$^+$podoplanin$^-$), which line the blood vessels (Fig. 3a). Both LECs and BECs have roles in immune cell recruitment through their expression of cell adhesion molecules and chemokines[35,36]. Examination of cell adhesion molecules expressed by LECs failed to show differences between LIF-cKO and control mice (Extended Data Fig. 6a). However, lung LECs expressed CCL21 (the ligand for CCR7) whereas BECs did not (Fig. 3b), and CCL21 increased during PVM infection (Extended Data Fig. 6b). In vitro expanded LECs responded to LIF by phosphorylation of STAT3 (Fig. 3c) and rapid upregulation of intracellular CCL21 (Fig. 3d), resulting in a 400-fold increase in secreted CCL21 (Fig. 3e). By contrast, LEC expression of chemokines CCL19, CCL25, CXCL9 and CXCL10 was either not detectable or not induced by LIF stimulation (Extended Data Fig. 6c). Intranasal administration of LIF to WT mice increased LEC expression of CCL21 (Fig. 3f) although it did not increase the total numbers of CCL21$^+$ LECs (Extended Data Fig. 6d). Notably, PVM-infected LIF-cKO mice had fewer CCL21-expressing LECs (Fig. 3g), which expressed fewer *Ccl21* transcripts than LEC from control mice (Fig. 3h). These data demonstrate that ILC2-derived LIF stimulates LECs to produce CCL21, a necessary cue for the efficient migration of CCR7$^+$ immune cells to LNs[17,18,37]. Indeed, the defect in CCL21 expression was associated with a deficit in CCR7$^+$ immune cells in the MedLN, but not lung, when LIF was deleted specifically in ILC2s (Fig. 3i and Extended Data Fig. 6e).

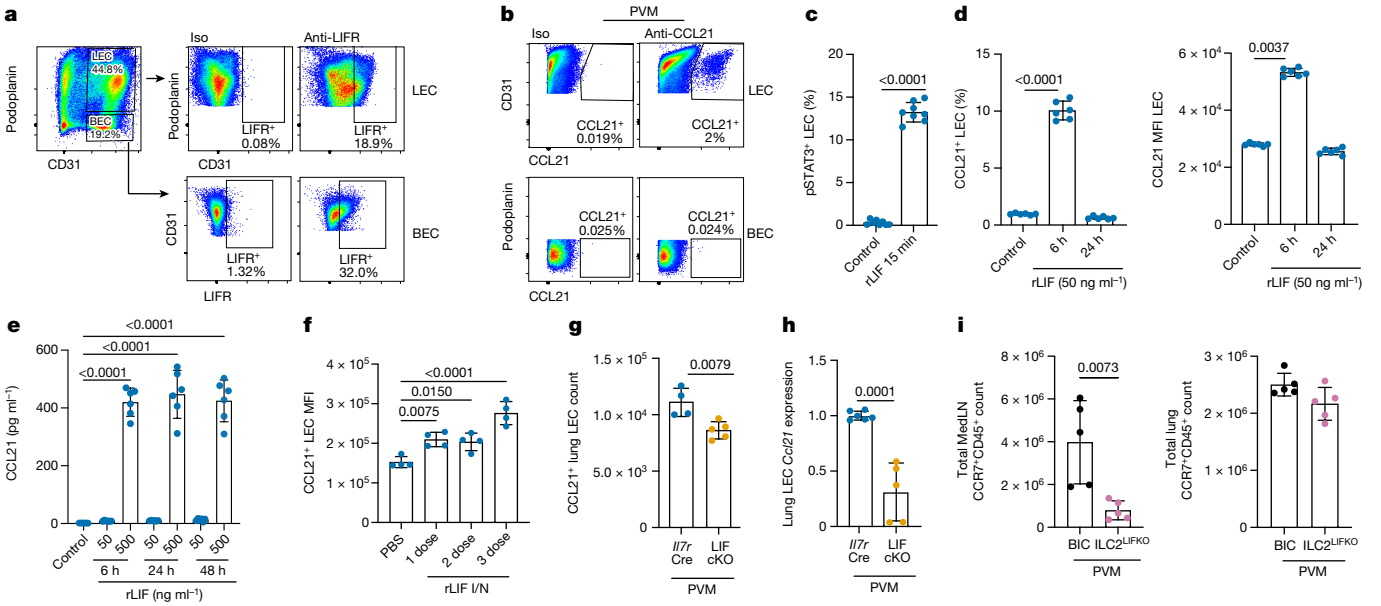

Fig. 3 | ILC2-derived LIF induces CCL21 production by LECs. a,**b**, Flow cytometry analysis of LIFR expression in lung LECs and BECs in naive mice (**a**) and CCL21 expression in lung LECs and BECs following PVM challenge (**b**). **c**,**d**, Flow cytometry analysis of phosphorylated STAT3$^+$ in cultured LECs following rLIF treatment (*Il7r*^{Cre}, $n = 8$; LIF-cKO, $n = 8$) (**c**) and CCL21$^+$ LEC percentage and CCL21 median fluorescence intensity (MFI) following rLIF treatment (*Il7r*^{Cre}, $n = 6$; LIF-cKO, $n = 6$) (**d**). **e**, ELISA of CCL21 concentration in in vitro cultured LEC-conditioned media following rLIF treatment (control, $n = 5$; rLIF, $n = 6$). **f**,**g**, Flow cytometry analysis of CCL21 MFI of lung LECs in WT mice following rLIF challenge at the indicated time points ($n = 4$) (**f**) and CCL21$^+$ lung LEC numbers in *Il7r*^{Cre} and LIF-cKO mice following PVM challenge (*Il7r*^{Cre}, $n = 4$; LIF-cKO, $n = 5$) (**g**). **h**, qPCR analysis of *Ccl21* relative expression in purified lung LECs from *Il7r*^{Cre} and LIF-cKO mice following PVM challenge (*Il7r*^{Cre}, $n = 6$; LIF-cKO, $n = 5$). **i**, Flow cytometry analysis of MedLN and lung CCR7$^+$CD45$^+$ cell numbers in BIC and ILC2^{LIFKO} mice following PVM challenge ($n = 5$). **c**,**d**,**f**–**i**, Unpaired two-sided *t*-test; **e**, one-way ANOVA with Tukey's multiple-comparisons test. Data presented as mean ± s.e.m. **a**–**d**,**f**–**i**, Data are representative of two independent experiments with similar results; **e**, experiments are pooled data from two independent experiments.

ILC2–LIF axis helps protect from viral reinfection

We next determined whether the defective primary immune response of LIF-cKO mice to viral infection could be overcome by secondary reinfection 30 days following the original viral challenge (Extended Data Fig. 7a). Despite comparable numbers of immune cells in the lungs of both LIF-cKO and control mice (Extended Data Fig. 7b), there was a marked deficit in the cellularity and immune cell composition in MedLN of LIF-cKO mice (Fig. 4a–f). This included fewer CD4$^+$ and CD8$^+$ T effector (T_{eff}, CD44^{hi}CD62L$^-$) cells, CD8$^+$ T central memory (T_{CM}, CD44^{hi}CD62L$^+$) cells, cDCs, pDCs and B cells (Fig. 4b–f and Extended Data Fig. 7c,d). B cell deficiency was reflected in a failure to upregulate the expression of circulating IgE (Fig. 4g), which is normally elevated in response to PVM infection[38,39]. Similarly, ILC2^{LIFKO} mice had fewer CD45$^+$ immune cells in their MedLN following PVM rechallenge (Extended Data Fig. 7e–g), including T_{eff} cells, T_{CM} cells, cDCs, pDCs and B cells in the MedLN (Extended Data Fig. 7h–l). A deficit in B cells also correlated with decreased circulating serum IgE (Extended Data Fig. 7m). Furthermore, whereas the secondary immune response cleared the virus from the lungs of control mice, the deficit in adaptive immunity in both LIF-cKO mice (Fig. 4h) and ILC2^{LIFKO} mice (Extended Data Fig. 7n) correlated with persistent viral infection. This was associated with reduced viral neutralization activity in the serum of both LIF-cKO (Fig. 4i) and ILC2^{LIFKO} mice (Extended Data Fig. 7o) as compared with controls. These results indicate that the generation of acquired immunity to PVM is impaired in the absence of ILC2-derived LIF.

LIF deficiency promotes allergen-induced iBALT

Finally we wondered how the LIF-dependent defect in immune cell homing would impact more chronic models of inflammatory disease, such as persistent type 2 allergen-induced inflammation used to model allergy and asthma[40]. Consequently we challenged LIF-cKO mice intranasally with RWP for 5 consecutive weeks (Extended Data Fig. 8a). Even following such protracted immune challenge, the levels of LIF were reduced in the lungs of LIF-cKO mice (Extended Data Fig. 8b). Histological analysis of lung from RWP-challenged LIF-cKO mice showed the formation of iBALT (Fig. 5a–c and Extended Data Fig. 8c,d), although lung eosinophils, neutrophils, alveolar macrophages and monocytes were unchanged (Extended Data Fig. 8e). iBALT associates with localized immune responses[15,41]. Fluorescent imaging confirmed T cells and B cells organized in regions rich in CD3$^-$KLRG1$^+$ILC2s and close to pulmonary lymphatic vessels, labelled with VEGFR3, in both LIF-cKO and ILC2^{LIFKO} mice (Fig. 5c and Extended Data Fig. 8f,g).

Notably, even after such sustained RWP antigen challenge, MedLNs were smaller in LIF-cKO mice due to a deficit in CD45$^+$ immune cells (Fig. 5d,e), including CD4$^+$ T_{eff} cells, CD4$^+$ T_{CM} cells, DCs and B cells in MedLN (but not in lung) as compared with controls (Fig. 5f–i and Extended Data Fig. 8h–l). Immunofluorescence staining of MedLN confirmed the difference in MedLN size (Fig. 5j), which suggested a potential impairment of adaptive immunity. Indeed, chronic RWP challenge of LIF-cKO mice led to considerably reduced circulating IgE compared with controls (Fig. 5k). In ILC2^{LIFKO} mice, lung eosinophils, neutrophils, alveolar macrophages and monocytes were unchanged (Extended Data Fig. 8m) but they showed reduced BAL LIF levels (Extended Data Fig. 8n) and fewer CD45$^+$ immune cells in their MedLN following chronic RWP challenge (Fig. 5l). A deficit in T_{eff} cells, T_{CM} cells, DCs and B cells in MedLN (Fig. 5m–q and Extended Data Fig. 8o), but not in the lungs (Extended Data Fig. 8p–s), correlated with a decrease in serum IgE (Fig. 5r). The inguinal LN, which does not drain the lung, showed no changes in cellularity following lung challenge, indicating that the effects of LIF deletion do not impact LNs not directly involved in the antigen-driven immune reaction (Extended Data Fig. 8t). These findings are in line with ILC2s continuing to be an indispensable source of LIF

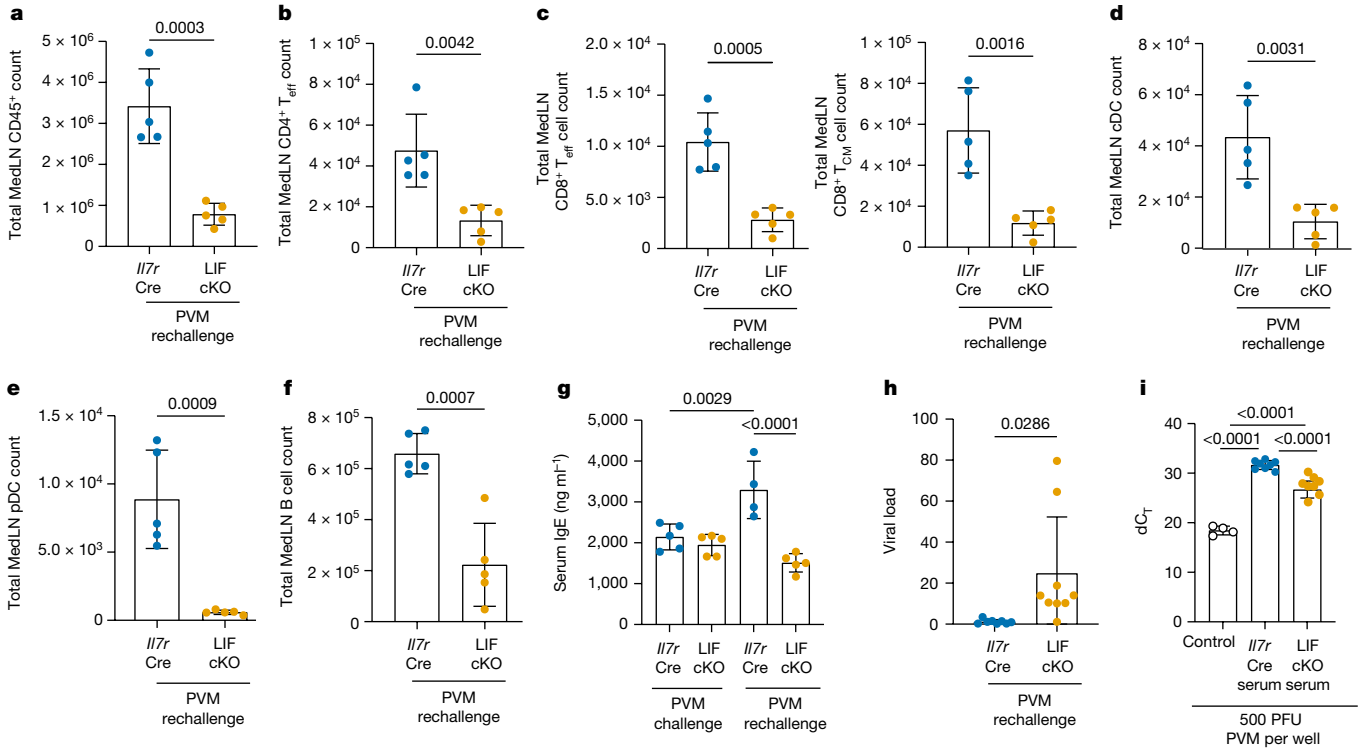

Fig. 4 | Defective immunity and MedLN colonization persist even following viral reinfection. a–**f**, Flow cytometry analysis of $CD45^+$ (**a**), $CD4^+T_{eff}$ cell (**b**), $CD8^+T_{eff}$ cell and T_{CM} cell (**c**), cDC (**d**), pDC (**e**) and B cell numbers (**f**) in *Il7r*^{Cre} and LIF-cKO mice following PVM rechallenge ($n = 5$). **g**, ELISA of serum IgE in *Il7r*^{Cre} and LIF-cKO mice following PVM primary (*Il7r*^{Cr}, $n = 5$; LIF-cKO, $n = 5$) and secondary (*Il7r*^{Cre}, $n = 4$; LIF-cKO, $n = 5$) challenge. **h**, Lung viral load in *Il7r*^{Cre} and LIF-cKO mice following PVM rechallenge (*Il7r*^{Cre}, $n = 8$; LIF-cKO, $n = 9$). **i**, In vitro viral neutralization assay with *Il7r*^{Cre} and LIF-cKO serum following PVM rechallenge. dC_T was calculated as C_T(PVM)-C_T (hamster GAPDH) (control, $n = 4$; PVM rechallenged *Il7r*^{Cre} serum, $n = 8$; PVM rechallenged LIF-cKO serum, $n = 8$). **a**–**f**,**h**,**i**, Unpaired two-sided *t*-test; **g**, one-way ANOVA with Tukey's multiple-comparisons test. Data presented as mean ± s.e.m. **a**–**g**,**i**, Data are representative of two independent experiments with similar results; **h**, experiments are pooled data from two independent experiments. PFU, plaque-forming units.

even following 5 weeks of antigen challenge (Extended Data Fig. 8u), although it is also possible that T cells may start to contribute as the response progresses. Finally, it is notable that the formation of iBALT in lung tissue did not rescue the deficit in total circulating serum IgE levels in either LIF-cKO or ILC2^{LIFKO} mice (Fig. 5r). Thus, responses to allergen in the absence of ILC2-derived LIF become amplified in the lung, leading to inappropriate tissue-localized iBALT reactions similar to those in asthma and allergy, but also to impaired systemic responses.

Discussion

Here we identified that LIF, produced by ILC2s, is essential for ensuring the efficient transition from lung tissue-localized immune reactions to LN-mediated systemic immunity. In the absence of ILC2-derived LIF, both antiviral and allergen-induced respiratory immune responses remained lung-centric with minimal immune cell seeding and expansion within draining LNs. This resulted in enhanced antiviral immunity but abnormal formation of iBALT in response to allergen challenge. We determined that LIF can both rapidly and directly promote CCR7 expression on pDCs and potently induce CCL21 chemokine production from $LIFR^+$ LECs to enhance $CCR7^+$ immune cell migration (including DCs and T cells) to the LNs to prime adaptive immunity (Extended Data Fig. 9). Indeed, conditional LIF deficiency closely phenocopies disruption of the CCR7–CCL21 chemokine pathway[15–18], which is critical for the trafficking of antigen-loaded DCs to LNs via the afferent lymphatics where they stimulate antigen-specific T cells to promote systemic immunity[17]. As a result, mice deficient in CCR7, CCL21 and CCL19, or following lung-specific ablation of CCL21-producing LECs, develop anomalous iBALT[15,17,18].

In the lungs, ILC2s and other lymphocytes commonly localize in the adventitial 'cuffs' within stromal niches close to lymphatic and blood vessels[28,42]. Here ILC2s sense stromal cell products or factors present in the fluid draining from the alveolar parenchyma to the lymphatics. These spatially restricted microenvironments leave ILC2s well placed to promote the local CCL21 chemokine gradients required to guide immune cell egress to the afferent lymphatics for transit to draining LNs[43,44]. Retention of DCs in the tissue would prolong their exposure to ILC2-derived cytokines such as GM-CSF, IL-4 and IL-13 (refs. 45,46), thereby locally activating DCs and promoting tissue-localized T cell responses[45–47]. Indeed, ILC2-derived IL-13 can stimulate DCs to produce the chemokine CCL17, which promotes the attraction of T_H2 cells[48]. In the absence of ILC2-produced LIF we did not observe excessive accumulation of immune cells in the lungs following viral or allergen challenge, presumably because fewer activated immune cells are generated in the LNs for release back into the blood circulation to traffic back to the lungs. Thus, inefficient cDC migration and tissue-localized T cell priming would promote dysregulated tertiary lymphoid structures to the detriment of normally coordinated systemic immunity in draining LNs.

iBALT is beneficial for focusing tissue-localized immune reactions against viral infection[17,18,37]. Although we did not find archetypal iBALT in the lungs of conditional LIF-deficient mice following PVM infection (which does not form chronic infections[38,39]), we observed increased cell aggregates and retention of pDCs in the lung. This correlated with increased type I IFN, improved viral clearance and a reduced type 2 response often associated with tissue repair. Indeed, LIF is required to protect the lungs of mice infected with RSV or challenged with *Escherichia coli*-induced pneumonia[49,50]. It will be interesting to determine whether ILC2-derived LIF also has roles during bacterial infections in

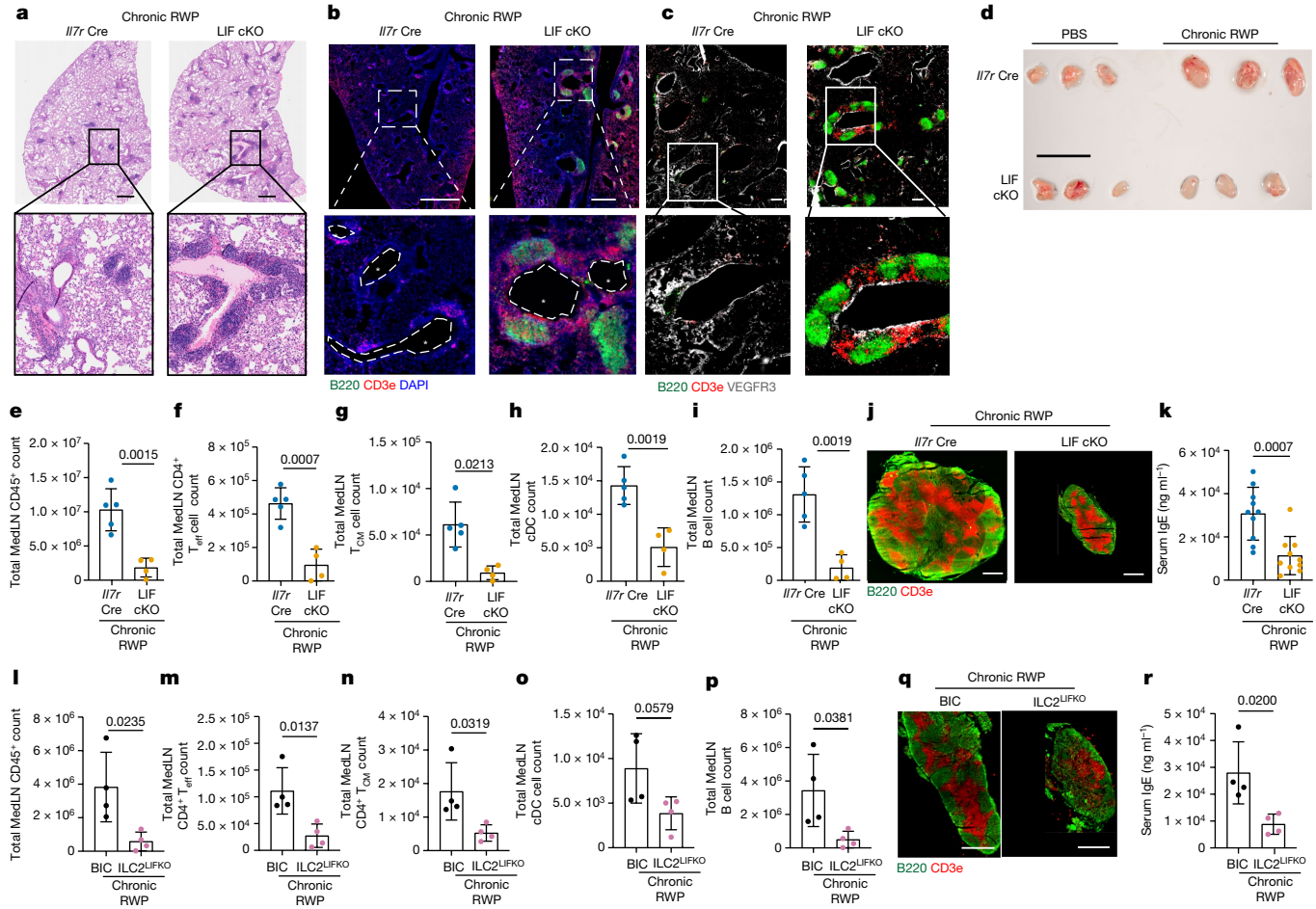

Fig. 5 | Chronic allergen challenge leads to marked iBALT accumulation in the absence of ILC2-derived LIF. a,**b**, Lung histology (**a**) and immunofluorescence (**b**) of *Il7r*^{Cre} and LIF-cKO mice following chronic RWP challenge. B cells were stained with B220 antibody (green), T cells with CD3e antibody (red) and nuclei with DAPI (blue). **c**, Immunofluorescence as in **b**, with B cells stained with B220 antibody (green), T cells with CD3e antibody (red) and lymphatic vessels with VEGFR3 (grey). **d**, Representative image of MedLN from *Il7r*^{Cre} and LIF-cKO mice following PBS or chronic RWP challenge. **e**–**i**, Flow cytometry analysis of numbers of CD45$^+$ cells (**e**), CD4$^+$ T_{eff} cells (**f**), CD4$^+$ T_{CM} cells (**g**), cDCs (**h**) and B cells (**i**) from *Il7r*^{Cre} and LIF-cKO mice following chronic RWP challenge (*Il7r*^{Cre}, $n = 5$; LIF-cKO, $n = 4$). **j**, Immunofluorescence of MedLN from *Il7r*^{Cre} and LIF-cKO mice following chronic RWP challenge. B cells were stained with B220 antibody (green) and T cells with CD3e antibody (red). **k**, ELISA of serum IgE from *Il7r*^{Cre} and LIF-cKO mice following chronic RWP challenge ($n = 10$). **l**–**p**, Flow cytometry analysis of CD45$^+$ cells (**l**), CD4$^+$ T_{eff} cells (**m**), CD4$^+$ T_{CM} cells (**n**), cDCs (**o**) and B cells (**p**) from BIC and ILC2^{LIFKO} mice following chronic RWP challenge ($n = 4$). **q**, Immunofluorescence of MedLN from BIC and ILC2^{LIFKO} mice following chronic RWP challenge. B cells were stained with B220 antibody (green) and T cells with CD3e antibody (red). **r**, ELISA of serum IgE from BIC and ILC2^{LIFKO} mice following chronic RWP challenge ($n = 4$). **e**–**i**,**k**–**p**,**r**, Unpaired two-sided *t*-test. Data presented as mean ± s.e.m. **a**–**j**,**l**–**r**, Data are representative of two independent experiments with similar results; **k**, experiments are pooled data from two independent experiments. Scale bars, 10 µm (**a**), 70 µm (**b**), 45 µm (**c**), 10 mm (**d**), 50 µm (**j**), 70 µm (**q**).

which pathogen-associated molecular pattern-driven immune activation is important. Because type I IFN can inhibit ILC2 functions[9,10] and LIF can suppress pDC production of type I IFN[25], this feedback mechanism may help to regulate the balance between antiviral type 1 immunity and reparative type 2 immunity to maintain, protect and restore lung health[9]. Indeed, dysregulated lung repair following primary infection may have contributed to the more persistent PVM virus infection we observed in response to PVM reinfection. Furthermore, ILC2-derived LIF was critical for establishing protective adaptive immunity to secondary infection with PVM virus, demonstrating the importance of the LIF signal in regulation of innate and acquired immunity.

iBALT formation also occurs with chronic allergen exposure, in which it is associated with detrimental lung inflammation[51]. Chronic allergen challenge of conditional LIF-deficient mice led to a pronounced and inappropriate accumulation of inflammatory cells in the lungs to form iBALT, to the detriment of draining LN responses. This failure of immune cells to move into the lymphatic system resulted in dysregulation of circulating IgE, an isotype indicative of atopic allergy and asthma-like responses[52]. This may be due directly to either impaired B cell migration or a shortfall in cDCs and T cells in the MedLN. Notably, mutations in the LIF receptor gene are associated with asthma in a population of Hutterites[53]. Although the authors did not investigate the mechanistic role of LIFR in asthma, the result raises the possibility that dysregulated LIFR signalling could contribute to abnormal immune cell homing in these individuals and contribute to symptoms. Also of note, RSV and influenza infection can exacerbate type 2-driven allergic asthma[14], highlighting the finely balanced regulation required in the lungs to avoid detrimental inflammatory responses.

Our results support a key role for ILC2-derived LIF in controlling immune cell migration from the lung to the MedLN following immune stimulation. This is, at least in part, due to potent regulation by LIF of the CCL21–CCR7 pathway, leading to phenotypes that closely resemble deletion of components of this chemokine axis. However, it remains possible that additional LIF-dependent signals are contributory and yet to be discovered. Nevertheless, our finding that ILC2-derived LIF is a previously unappreciated regulator of immune cell trafficking raises

fundamental questions about the role of this cytokine in human allergic disease and infections, but also in a broad range of other diseases—for example, inflammatory bowel disease and cancer in which intratumoural TLS[54] correlate with low LIF expression and may represent a positive prognostic indicator for certain cancers[55].

Online content

Any methods, additional references, Nature Portfolio reporting summaries, source data, extended data, supplementary information, acknowledgements, peer review information; details of author contributions and competing interests; and statements of data and code availability are available at https://doi.org/10.1038/s41586-024-07746-w.

1. Arasa, J., Collado-Diaz, V. & Halin, C. Structure and immune function of afferent lymphatics and their mechanistic contribution to dendritic cell and T cell trafficking. *Cells* https://doi.org/10.3390/cells10051269 (2021).
2. Griffith, J. W., Sokol, C. L. & Luster, A. D. Chemokines and chemokine receptors: positioning cells for host defense and immunity. *Annu. Rev. Immunol.* **32**, 659–702 (2014).
3. Rodriguez-Rodriguez, N., Gogoi, M. & McKenzie, A. N. J. Group 2 innate lymphoid cells: team players in regulating asthma. *Annu. Rev. Immunol.* **39**, 167–198 (2021).
4. Clementi, N. et al. Viral respiratory pathogens and lung injury. *Clin. Microbiol. Rev.* https://doi.org/10.1128/CMR.00103-20 (2021).
5. Molofsky, A. B. & Locksley, R. M. The ins and outs of innate and adaptive type 2 immunity. *Immunity* **56**, 704–722 (2023).
6. Castellanos, J. G. & Longman, R. S. The balance of power: innate lymphoid cells in tissue inflammation and repair. *J. Clin. Invest.* **129**, 2640–2650 (2019).
7. Monticelli, L. A. et al. Innate lymphoid cells promote lung-tissue homeostasis after infection with influenza virus. *Nat. Immunol.* **12**, 1045–1054 (2011).
8. Han, M. et al. The innate cytokines IL-25, IL-33, and TSLP cooperate in the induction of type 2 innate lymphoid cell expansion and mucous metaplasia in rhinovirus-infected immature mice. *J. Immunol.* **199**, 1308–1318 (2017).
9. Duerr, C. U. et al. Type I interferon restricts type 2 immunopathology through the regulation of group 2 innate lymphoid cells. *Nat. Immunol.* **17**, 65–75 (2016).
10. Moro, K. et al. Interferon and IL-27 antagonize the function of group 2 innate lymphoid cells and type 2 innate immune responses. *Nat. Immunol.* **17**, 76–86 (2016).
11. Vu, L. D. et al. Elevated levels of type 2 respiratory innate lymphoid cells in human infants with severe respiratory syncytial virus bronchiolitis. *Am. J. Respir. Crit. Care Med.* **200**, 1414–1423 (2019).
12. Li, B. W. S. et al. T cells and ILC2s are major effector cells in influenza-induced exacerbation of allergic airway inflammation in mice. *Eur. J. Immunol.* **49**, 144–156 (2019).
13. Sposito, B. et al. The interferon landscape along the respiratory tract impacts the severity of COVID-19. *Cell* **184**, 4953–4968 (2021).
14. Wu, W. & Metcalf, J. P. The role of type I IFNs in influenza: antiviral superheroes or immunopathogenic villains? *J. Innate Immun.* **12**, 437–447 (2020).
15. Fleige, H. et al. Manifold roles of CCR7 and its ligands in the induction and maintenance of bronchus-associated lymphoid tissue. *Cell Rep.* **23**, 783–795 (2018).
16. Grinnan, D. et al. Enhanced allergen-induced airway inflammation in paucity of lymph node T cell (plt) mutant mice. *J. Allergy Clin. Immunol.* **118**, 1234–1241 (2006).
17. Gunn, M. D. et al. Mice lacking expression of secondary lymphoid organ chemokine have defects in lymphocyte homing and dendritic cell localization. *J. Exp. Med.* **189**, 451–460 (1999).
18. Forster, R. et al. CCR7 coordinates the primary immune response by establishing functional microenvironments in secondary lymphoid organs. *Cell* **99**, 23–33 (1999).
19. Kallal, L. E., Hartigan, A. J., Hogaboam, C. M., Schaller, M. A. & Lukacs, N. W. Inefficient lymph node sensitization during respiratory viral infection promotes IL-17-mediated lung pathology. *J. Immunol.* **185**, 4137–4147 (2010).
20. Marin, N. D., Dunlap, M. D., Kaushal, D. & Khader, S. A. Friend or foe: the protective and pathological roles of inducible bronchus-associated lymphoid tissue in pulmonary diseases. *J. Immunol.* **202**, 2519–2526 (2019).
21. Barlow, J. L. et al. IL-33 is more potent than IL-25 in provoking IL-13-producing nuocytes (type 2 innate lymphoid cells) and airway contraction. *J. Allergy Clin. Immunol.* **132**, 933–941 (2013).
22. Oboki, K. et al. IL-33 is a crucial amplifier of innate rather than acquired immunity. *Proc. Natl Acad. Sci. USA* **107**, 18581–18586 (2010).
23. Swiecki, M. & Colonna, M. The multifaceted biology of plasmacytoid dendritic cells. *Nat. Rev. Immunol.* **15**, 471–485 (2015).
24. Wendland, M. et al. CCR9 is a homing receptor for plasmacytoid dendritic cells to the small intestine. *Proc. Natl Acad. Sci. USA* **104**, 6347–6352 (2007).
25. Sesti-Costa, R. et al. Leukemia inhibitory factor inhibits plasmacytoid dendritic cell function and development. *J. Immunol.* **204**, 2257–2268 (2020).
26. Abbas, A. et al. The activation trajectory of plasmacytoid dendritic cells in vivo during a viral infection. *Nat. Immunol.* **21**, 983–997 (2020).
27. Nicola, N. A. & Babon, J. J. Leukemia inhibitory factor (LIF). *Cytokine Growth Factor Rev.* **26**, 533–544 (2015).
28. Dahlgren, M. W. et al. Adventitial stromal cells define group 2 innate lymphoid cell tissue niches. *Immunity* **50**, 707–722 (2019).
29. Debes, G. F. et al. Chemokine receptor CCR7 required for T lymphocyte exit from peripheral tissues. *Nat. Immunol.* **6**, 889–894 (2005).
30. Seth, S. et al. CCR7 essentially contributes to the homing of plasmacytoid dendritic cells to lymph nodes under steady-state as well as inflammatory conditions. *J. Immunol.* **186**, 3364–3372 (2011).
31. Davidson, S. et al. Plasmacytoid dendritic cells promote host defense against acute pneumovirus infection via the TLR7-MyD88-dependent signaling pathway. *J. Immunol.* **186**, 5938–5948 (2011).
32. Garvey, T. L. et al. Inflammatory responses to pneumovirus infection in IFN-alpha beta R gene-deleted mice. *J. Immunol.* **175**, 4735–4744 (2005).
33. Szeto, A. C. H. et al. Mef2d potentiates type-2 immune responses and allergic lung inflammation. *Science* https://doi.org/10.1126/science.adl0370 (2024).
34. Varese, A. et al. Type I interferons and MAVS signaling are necessary for tissue resident memory $CD8^+$ T cell responses to RSV infection. *PLoS Pathog.* **18**, e1010272 (2022).
35. Jalkanen, S. & Salmi, M. Lymphatic endothelial cells of the lymph node. *Nat. Rev. Immunol.* **20**, 566–578 (2020).
36. Farnsworth, R. H., Karnezis, T., Maciburko, S. J., Mueller, S. N. & Stacker, S. A. The interplay between lymphatic vessels and chemokines. *Front. Immunol.* **10**, 518 (2019).
37. Mori, S. et al. Mice lacking expression of the chemokines CCL21-ser and CCL19 (plt mice) demonstrate delayed but enhanced T cell immune responses. *J. Exp. Med.* **193**, 207–218 (2001).
38. Siegle, J. S. et al. Early-life viral infection and allergen exposure interact to induce an asthmatic phenotype in mice. *Respir. Res.* **11**, 14 (2010).
39. Kaiko, G. E. et al. Toll-like receptor 7 gene deficiency and early-life Pneumovirus infection interact to predispose toward the development of asthma-like pathology in mice. *J. Allergy Clin. Immunol.* **131**, 1331–1339 (2013).
40. Kerscher, B. et al. BET bromodomain inhibitor iBET151 impedes human ILC2 activation and prevents experimental allergic lung inflammation. *Front. Immunol.* **10**, 678 (2019).
41. Matsumoto, R. et al. Induction of bronchus-associated lymphoid tissue is an early life adaptation for promoting human B cell immunity. *Nat. Immunol.* **24**, 1370–1381 (2023).
42. Dahlgren, M. W. & Molofsky, A. B. Adventitial cuffs: regional hubs for tissue immunity. *Trends Immunol.* **40**, 877–887 (2019).
43. Moore, J. E. Jr., Brook, B. S. & Nibbs, R. J. B. Chemokine transport dynamics and emerging recognition of their role in immune function. *Curr. Opin. Biomed. Eng.* **5**, 90–95 (2018).
44. Weber, M. et al. Interstitial dendritic cell guidance by haptotactic chemokine gradients. *Science* **339**, 328–332 (2013).
45. Piemonti, L. et al. IL-13 supports differentiation of dendritic cells from circulating precursors in concert with GM-CSF. *Eur. Cytokine Netw.* **6**, 245–252 (1995).
46. Jared Brooksby, T. K., Iijima, K., Lama, J. & Kita, H. Group 2 innate lymphoid cells are involved in development of antigen-specific Th2 cells by providing GM-CSF and activating dendritic cells. *J. Allergy Clin. Immunol.* https://doi.org/10.1016/j.jaci.2022.12.008 (2023).
47. Chi, L. et al. Sexual dimorphism in skin immunity is mediated by an androgen-ILC2-dendritic cell axis. *Science* https://doi.org/10.1126/science.adk6200 (2024).
48. Halim, T. Y. et al. Group 2 innate lymphoid cells license dendritic cells to potentiate memory TH2 cell responses. *Nat. Immunol.* **17**, 57–64 (2016).
49. Foronjy, R. F., Dabo, A. J., Cummins, N. & Geraghty, P. Leukemia inhibitory factor protects the lung during respiratory syncytial viral infection. *BMC Immunol.* **15**, 41 (2014).
50. Quinton, L. J. et al. Leukemia inhibitory factor signaling is required for lung protection during pneumonia. *J. Immunol.* **188**, 6300–6308 (2012).
51. Luo, S. et al. Chronic inflammation: a common promoter in tertiary lymphoid organ neogenesis. *Front. Immunol.* **10**, 2938 (2019).
52. Froidure, A. et al. Asthma phenotypes and IgE responses. *Eur. Respir. J.* **47**, 304–319 (2016).
53. Kurz, T. et al. Fine mapping and positional candidate studies on chromosome 5p13 identify multiple asthma susceptibility loci. *J. Allergy Clin. Immunol.* **118**, 396–402 (2006).
54. Loriot, Y. et al. Plasma proteomics identifies leukemia inhibitory factor (LIF) as a novel predictive biomarker of immune-checkpoint blockade resistance. *Ann. Oncol.* **32**, 1381–1390 (2021).
55. Zhang, Q. & Wu, S. Tertiary lymphoid structures are critical for cancer prognosis and therapeutic response. *Front. Immunol.* **13**, 1063711 (2022).

Methods

Mice

All mice were maintained in the Medical Research Council ARES animal facility under specific-pathogen-free conditions at 19–23 °C and 45–65% humidity with a 12/12 h light/dark cycle. In individual experiments, mice were matched for age, sex and background strain. All experiments undertaken in this study were performed with the approval of the LMB Animal Welfare and Ethical Review Body and the UK Home Office. C57BL/6 JOla controls were bred in house. Mouse strains *Il7r*^{Cre} (ref. 56), *Rora*$^{flox/flox}$ (ref. 57), *Il1rl1*$^{-/-}$ (ref. 58), *Rag2*$^{-/-}$, *Rag2*$^{-/-}$*Il2rgc*$^{-/-}$ (*Rag2*$^{-/-}$*gc*$^{-/-}$), *Lif*$^{flox/flox}$, BIC[33], *Siglech*^{Cre} (ref. 59) and *Lifr*$^{-/flox}$ were either on the C57BL/6J Ola background or back-crossed for at least six generations.

Generation of *Lif*$^{flox/flox}$ mice

To produce a *Lif* allele that could be conditionally deleted by Cre recombinase, we generated a homology-directed repair-template construct for use in combination with CRISPR–Cas9 to insert LoxP sites 5′ and 3′ of the final exon of both protein-coding annotated *Lif* transcripts (ENSMUSE00000656154). In addition, the construct included a neomycin selection cassette flanked by Frt sites to permit Flp-mediated excision, and both LoxP sites were followed by a BglII site to facilitate screening and verification of appropriately targeted embryonic stem cell clones (Extended Data Fig. 1r). Embryonic stem cells were transfected with this repair-template construct along with expression constructs for WT Cas9 and four single-guide RNAs, two targeting sequences 5′ and two targeting 3′ of the final *Lif* exon. Neomycin-resistant clones were screened for correct targeting initially by PCR and digested with BglII using 5′ primer pairs P1 and P2 such that a product cleaved by BglII indicated correct targeting. Clones were further verified by Southern blot analysis using 5′ and 3′ probes that both detected a 16.4 kb fragment in the WT allele and 4.9 and 7.6 kb fragments, respectively, in the targeted allele (Extended Data Fig. 1s). Guide RNA target sequences were: G1 (F) TAATGATTCTAGTTGCCTACAGG; G2 (F) TGGAGTCCCC ATGTCACAGGTGG; G3 (F) TTCCTCCATCGGTCCAGGAGGGG; G4 (R) TACCCCTCCTGGACCGATGGAGG. Screening primers were: P1 TAGGAAG CCAGAGTCTAGTGGCAGTTTTAAGAGATGG; P2 AAGGCTTCTTTGTCAG AGTGGTCGG. Primers for generation of probes were: 5′ probe 1 fwd CCTG CCACCCCCTTAACCTCCATAAGTGAAAAGCAAGTGG; 5′ probe 1 rev. ACTGGGCCTGCTAGGGGTTTGACAG; 3′ probe 1 fwd TGATGGAGCTGT GGGATGGG; 3′ probe 1 rev. ACACACTCGGGCTCCATTATGC.

Generation of LIFR conditional mice

For generation of pDC-specific LIFR knockout (*SiglecH*$^{Cre/Cre}$ *Lifr*$^{-/flox}$) mice, pDC^{Cre} (*SiglecH*$^{Cre/Cre}$) mice were crossed with *Lifr*$^{-/flox}$ to delete exon 5 of *Lifr* (transcript variant 1). Both Tg(Siglech-Cre,-mCherry)[59] and Lifr$^{tm1a(EUCOMM)Hmgu}$ (ref. 25) mice were obtained from the European mouse mutant archive. To delete the lacZ–neomycin-resistance cassette and generate mice with a *lox*P-flanked *Lifr* allele (EuComm *Lifr*^{tm1c} is denoted as *Lifr*^{flox} in this paper), chimaeras were bred to FLPe C57BL/6 mice. However, we also detected inefficient *Lifr*^{flox} allele recombination and consequently analysed pDC^{Cre} × *Lifr*$^{-/flox}$ mice in which two Cre-mediated recombination events occurred to produce LIFR deficiency, with pDC^{Cre} × *Lifr*$^{-/+}$ mice as controls. Despite two Cre alleles and one functional flox allele, pDC^{Cre} × *Lifr*$^{-/flox}$ mice showed a reduction in LIFR expression of only 50% in pDCs (Extended Data Fig. 1t).

Mouse challenge protocols

IL-33-induced type 2 lung inflammation. Mice were challenged intranasally with IL-33 (Biolegend; 0.25 μg in 40 μl of PBS) on 3 consecutive days. All tissues were harvested 24 h following the final dose.

Neutralizing LIF antibody treatment. Mice were intranasally challenged with IL-33 (0.25 μg in 40 μl of PBS) and intraperitoneally injected with 100 μg of either isotype antibody (R&D systems) or anti-LIF neutralizing antibody (R&D systems) on 3 consecutive days. All tissues were harvested 24 h following the final dose.

rLIF intranasal challenge. Mice were intranasally challenged with rLIF (R&D systems; 1 μg in 40 μl of PBS) on 3 consecutive days. All tissues were harvested 24 h following the final dose. For the pDC migration kinetics experiment, mice were intranasally challenged with one rLIF dose (1 μg in 40 μl of PBS) and tissues harvested at 6 or 24 h after challenge.

RWP-induced type 2 lung inflammation. Mice were intranasally challenged with RWP (300 μg of protein per dose, *Ambrosia artemisiifolia*, short form; Greer Laboratories) on 3 consecutive days. All tissues were harvested 24 h following the final dose. For the chronic lung inflammation model, mice were intranasally challenged with RWP thrice weekly over 5 weeks. All tissues were harvested on day 38.

FITC-dextran-labelled cell migration. Mice were challenged intranasally with IL-33 (Biolegend, 0.25 μg) and 40 kDa FITC-dextran (Sigma-Aldrich, 40 μg in 50 μl of PBS) on 3 consecutive days. All tissues were harvested 24 h following the final dosing.

Mouse infection models

PVM infection. Mice were infected intranasally with a single dose of PVM (50 PFU in PBS). PVM strain J3666 stock was a gift from A. J. Easton. All tissues were harvested at 8 days postinfection unless stated otherwise. For the CCL21 kinetics experiment, mice were intranasally challenged with PVM (50 PFU in PBS) and tissues harvested on 0, 4, 8 and 11 days postinfection.

For PVM rechallenge, mice were challenged with PVM (50 PFU in PBS) on days 0 and 30 and all tissues were harvested on day 38.

FITC-dextran-labelled cell migration. Mice were challenged intranasally with PVM (50 PFU) and 40 kDa FITC-dextran (Sigma-Aldrich, 40 μg in 50 μl of PBS). All tissues were harvested 3 days postinfection.

rLIF and PVM challenge. Mice were infected with a single dose of PVM (50 PFU in PBS) intranasally and treated with a daily dose of intranasal rLIF(1 μg) or PBS. All tissues were harvested on day 8 postinfection.

Mice were infected with a single dose of PVM (50 PFU in PBS) intranasally and, on day 8, postinfection intravenous CD45 labelling was performed by injection of 3 μg of anti-CD45 antibody (in 200 μl of PBS) via the tail vein. Mice were then culled 3 min after injection and tissues harvested.

FTY720 and PVM challenge. Mice were infected with a single dose of PVM (50 PFU in PBS) intranasally and injected intraperitoneally daily with either FTY720 (ref. 34) (25 μg in 250 μl; Enzo Life Sciences) or PBS. All tissues were harvested on day 8 postinfection.

Tissue processing

BAL isolation. Mice were culled at the experimental endpoint, tracheae were exposed and BAL was performed by flushing the lungs three times with 0.5 ml of PBS. The fluid obtained was centrifuged at 350*g* for 5 min; supernatants were stored at −20 °C for cytokine detection.

Serum isolation. Mice were culled at the experimental endpoint and whole blood was collected. Blood samples were allowed to clot for 2 h at room temperature. Samples were centrifuged at 2,000*g* for 10 min and serum was collected and stored at −20 °C. For immunoglobulin enzyme-linked immunosorbent assay (ELISA), serum was diluted 1/50.

Viral load. Mice were culled at the experimental endpoint, and one lung lobe was snap-frozen in trizol (Invitrogen) and stored at −80 °C for RNA purification.

Tissue preparation. Lung tissue was predigested with 750 U ml^{-1} collagenase I (Gibco) and 0.3 mg ml^{-1} DNase I (Sigma-Aldrich) before obtaining a single-cell suspension at 37 °C for 30 min; tissue was then passed through a 70 µm cell strainer. For lymphocyte enrichment, a single-cell lung suspension was centrifuged through 30% Percoll (GE Healthcare) at 800*g* for 15 min. Spleen, thymus and mediastinal LN single-cell suspensions were prepared by passing tissue through a 70 µm cell strainer and lysing red blood cells. Single-bone marrow cell suspensions were prepared by flushing the femur and tibia with endotoxin-free PBS and lysing red blood cells.

Flow cytometry

Single-cell suspensions were incubated with fluorochrome- or biotin-conjugated antibodies in the presence of anti-CD16/CD32 antibody (Fc block, clone 2.4G2), followed by fluorochrome-conjugated streptavidin where necessary. All samples were costained with a cell viability dye (Fixable dye eFluor780, Invitrogen) and analysed on either a 5-5-laser LSRFortessa system (BD Biosciences, BD FACSDiva software v.6.2) or spectral cytometer ID7000 (Sony Biotechnology). Either FACSAria Fusion systems or iCyt Synergy (70 µm nozzle, Sony Biotechnology) was used for cell sorting. Precision Count Beads (BioLegend) were used to calculate cell numbers. Intracellular transcription factor staining was performed using the Foxp3 staining kit (eBioscience) according to the manufacturer's instructions. For lymphocyte intracellular cytokine staining, cells were cultured with complete RPMI supplemented with Cell Stimulation Cocktail or protein transport inhibitors (eBioscience) for 4 h at 37 °C. Intracellular cytokine staining was performed using BD Cytofix/Cytoperm Plus reagents (BD Biosciences) following the manufacturer's instructions. The expression of LEC CCL21 was detected by additional staining with goat anti-mouse CCL21 (R&D systems) and anti-goat-Alexa 488 (Invitrogen), with no stimulation, and using BD Cytofix/Cytoperm Plus reagents (BD Biosciences) following the manufacturer's instructions.

For intracellular phospho-STAT3 staining, cells were fixed with 2% paraformaldehyde (PFA) for 15 min and overnight permeabilization with 90% methanol at −20 °C, followed by incubation with fluorochrome antibodies diluted in 2% bovine serum albumin PBS.

Flow cytometric analysis, including unsupervised dimensionality reduction and clustering, was performed using FlowJo, LLC v.10 (BD) and associated plug-ins. Unless otherwise stated, pDCs are defined as LiveCD45$^+$CD11b$^-$F4/80$^-$CD317$^+$SiglecH$^+$. Myeloid cells include cDCs and CD11b$^-$ cDCs as LiveCD45$^+$CD11b$^-$CD11c^{high}SiglecF$^-$MHCII^{high}; CD11b$^+$ cDCs as LiveCD45$^+$CD11c$^{-/int}$ SiglecF$^-$Ly6G$^-$CD19$^-$TCRb$^-$MHCII^{high}; monocytes as LiveCD45$^+$CD11b$^+$ SiglecF$^-$Ly6G$^-$F4/80$^+$MHCII$^-$; and alveolar macrophages as CD45$^+$CD11c$^+$F4/80$^+$SiglecF$^+$. Eosinophils are defined as CD45$^+$CD11c$^-$F4/80$^-$CD11b$^+$Gr1^{int} SiglecF$^+$; and neutrophils as CD45$^+$CD11c$^-$F4/80$^-$CD11b$^+$Ly6G^{high}SiglecF$^-$. T cells are defined as LiveCD45$^+$TCRb$^+$ and B cells as LiveCD45$^+$CD19$^+$TCRb$^-$; CD4$^+$ T cells as CD45$^+$CD3$^+$CD4$^+$ and ILC2s as CD45$^+$Lin$^-$(CD3,CD4, CD8,CD19,CD11b,CD11c,FcεR1) CD127$^+$ICOS$^+$. Endothelial cells are defined as LiveCD45$^-$CD31$^+$, LECs as LiveCD45$^-$CD31$^+$PDPN$^+$ and BECs as LiveCD45$^-$CD31$^+$ PDPN$^-$.

All flow cytometry data were processed and analysed using FlowJo v.10, RRID: https://scicrunch.org/resolver/SCR_008520.

In vitro cultured cells

Lung immune cell sorting. Mouse ILC2s were purified from IL-33-treated lungs (see Methods for IL-33-induced type 2 lung inflammation) as LiveCD45$^+$Lineage$^-$IL-7Rα$^+$ST2$^+$KLRG1$^+$; and pDCs were purified from IL-33-treated lungs (see Methods for IL-33-induced type 2 lung inflammation) as LiveCD45$^+$F4/80$^-$CD11b$^-$CD317$^+$SiglecH. Cells were snap-frozen in trizol for RNA purification, and conditioned medium was collected and stored at −20 °C.

Mouse lung ILC2s and T cells for qPCR analysis were purified from PVM-challenged mice using the same gating strategy as for ILC2s: LiveCD45$^+$Lineage$^-$IL-7Rα$^+$ST2$^+$KLRG1$^+$; CD4$^+$ T cells as LiveCD45$^+$TCRb$^+$CD4$^+$; CD8$^+$ T cells as LiveCD45$^+$TCRb$^+$CD8$^+$; BECs as LiveCD45$^-$CD31$^+$PDPN$^-$; and LECs as LiveCD45$^-$CD31$^+$PDPN$^+$. Purified cells were snap-frozen in trizol for RNA purification.

ILC2 in vitro stimulation. Purified ILC2s were cultured for 24 h with IL-7 (10 ng ml^{-1}) and IL-2 (50 ng ml^{-1}) with or without IL-33 (10 ng ml^{-1}). Cells for RNA purification and conditioned media were collected and stored at −20 °C.

pDC culture, purification and activation. Bone marrow cells were obtained by flushing femurs and tibias with RPMI, followed by incubation with red blood cell lysis buffer for 5 min. Following washing, cells were cultured with RPMI containing 10% fetal calf serum, 1% penicillin/streptomycin, sodium pyruvate, non-essential amino acids, L-glutamine, β-mercaptoethanol and Flt3L (10 ng ml^{-1}) for 7–10 days. Medium was refreshed on days 3 and 6. pDCs were sorted from bone marrow-derived cultures by fluorescent activated cell sorting as LiveCD45$^+$CD11c^{int}SiglecH$^+$CD317$^+$ cells. Purified pDCs were activated with CpG (6 µg ml^{-1}, Invivogen) and treated with or without rLIF (500 ng ml^{-1}) for 24 h.

Chemotaxis assay. Migration assays were performed using Millicell cell culture inserts (Merck Millipore) with 2–3 × 10^5 cells per well. Purified pDCs were activated with CpG (6 µg ml^{-1}) and treated with or without rLIF (10 ng ml^{-1}) for 24 h. Activated pDCs were placed in inserts with 5 µm pores for 3 h in the presence or absence of cytokine rLIF (500 or 1000 ng ml^{-1}) or chemokine rCCL21 (R&D systems) at 150 ng ml^{-1}. The number of migrating cells was then evaluated using a flow cytometer. The results are expressed as migration index (number of migrating cells in chemokine/number of migrating cells in medium).

Lung LEC purification and culture

The preparation of single-cell suspensions from lung tissues is described in 'Tissue preparation'. CD31$^+$ lung cells were isolated from lung cell suspension using magnetic beads (CD31 biotin, Streptavidin dynabeads)[60]. Isolated CD31$^+$ lung cells were seeded onto 0.2% gelatin-coated, six-well plates and cultured on complete growth medium. consisting of ECGS (Corning), 20% fetal bovine serum, 1% penicillin/streptomycin, sodium pyruvate, non-essential amino acids and 25 mM HEPES, in a humidified incubator with a gas mixture of 21% O_2 and 5% CO_2 at 37 °C until 70–80% confluence was achieved (usually reached in 4–7 days). Endothelial cells were detached with Accutase (Stemcell Technologies) and purified using magnetic beads (podoplanin biotin, Streptavidin dynabeads). Purified LECs were seeded onto 0.2% gelatin-coated, six-well plates, cultured in complete growth medium and used for experiments.

In vitro LEC treatment

Isolated LECs were treated with or without rLIF for 6 or 24 h, detached using Accutase and stained for flow cytometry analysis.

ELISA and MAGPIX Luminex Array

Culture supernatant was collected and stored at −20 °C until analysis. Serum IgE was measured by ELISA (Invitrogen). LIF, IL-5, type I IFN, CCL19, CCL21, CCL25, CXCL9 and CXCL10 were measured using ProcartaPlex kits (Invitrogen).

Virus neutralization assay

Sera from PVM-rechallenged mice were diluted in a 1:10 ratio and heat-inactivated at 55 °C for 30 min. An equal volume of PVM at 500 PFU per well concentration (1:20 final serum dilution) was incubated with serum for 1 h at 37 °C and 5% CO_2. BHK-21 cell monolayers (1 × 10^5 per well) were infected with the virus mixture and incubated for 72 h at 37 °C and 5% CO_2. Before harvesting the cells were washed three times

with PBS, snap-frozen in Trizol (Invitrogen) and stored at −80 °C for RNA purification.

qPCR with reverse transcription

RNA was purified using Direct-zol RNA Purification Kits. For assessment of viral load, frozen tissue samples were homogenized before RNA purification. Complementary DNA synthesis was performed using SuperScript IV Reverse Transcriptase and oligo $d(T)_{20}$ (Invitrogen). PVM viral load was tested with forward primer 5′-GCCTGCATCAACACAGTGTGT and reverse primer 5′-GCCTGATGTGGCAGTGCTT[38] in a SYBR green qPCR assay. For lung samples, the mouse HPRT gene was used as an internal control. For the PVM neutralization assay, the dC_T for viral amplification was measured with respect to the hamster GAPDH gene. For other qPCR analyses, commercially available Taqman gene expression assays (Applied Biosystems; Extended Data Table 1) were used. Samples were run on the ViiA7 real-time PCR system (Applied Biosystems).

RNA-seq

Cells were sorted by flow cytometry into PBS and 50% fetal calf serum. and RNA was extracted using the RNeasy Plus Micro kit (Qiagen). Following assessment using a Bioanalyser (Agilent), RNA was processed for RNA-seq using Ovation RNA-seq System v.2 (Nugen), fragmented by a Covaris M220 ultrasonicator and bar-coded using Ovation Ultralow Library Systems (Nugen). Samples were sequenced using an Illumina HiSeq 4000 by running a single-read 50-base-pair protocol (Cancer Research UK, Cambridge Institute). Sequence data were trimmed to remove adaptors and sequences with a quality score below 30 using Trim Galore (v.0.50, Babraham Bioinformatics) and then aligned to the mouse genome (GRCm38) using STAR (v.2.6.0a); differential expression was calculated using DESeq2 (v.1.18.1).

Bioinformatic identification of candidate ligands and receptor pairs

Gene lists for cytokines and cytokine receptors were obtained by downloading Gene Ontology gene lists for 'Cytokine Activity' and 'Cytokine Receptor Activity' from the Mouse Genome Informatics website. The curated mouse CellTalkDB database of ligand–receptor pairs was used to identify interacting gene pairs between these gene lists[61]. Using R programming language, the dplyr package was utilized to filter the CellTalkDB database by the cytokine and cytokine receptor gene lists to remove non-cytokine-related ligand–receptor pairs. This filtered list of ligand–receptor pairs was then used to interrogate bulk RNA-seq data of pDCs and ILC2s isolated from mouse lung. Expression of cytokine ligand–receptor pairs in which expression of the receptor by pDCs was greater than 10 RPMK and expression of the ligand by ILC2s was greater than 10 RPKM was then extracted. Ligand–receptor pairs involving *Cd44* or *Cd74* were excluded from the analysis due to the high expression levels of these transcripts.

Histology

Tissue was fixed in 10% formalin overnight and paraffin embedded; sections were stained with haematoxylin and eosin. Lung histology sections were assessed by a researcher blinded to groupings and given a score between 0 and 5 based on the presence or absence of large cellular aggregates.

Microscopy

Mice were euthanized and received intracardiac perfusion with PBS, followed by 4% PFA (Invitrogen). Lung and LN were collected and fixed with 4% PFA overnight. Fixed tissues were washed with PBS and placed in 30% sucrose for 24 h. Subsequently these were embedded in Optimum Cutting Temperature compound (VWR, catalogue no. 25608-930), frozen in Isopentane and sectioned on a Leica CM1860 cryostat. Sections were incubated in a blocking solution (2% goat serum and 0.5% Triton X-100 in PBS) for 1 h at room temperature. Tissue sections were then incubated overnight at 4 °C with primary antibodies against CD3e, B220 and VEGFR3, then with secondary antibodies for 1 h at room temperature. Images were acquired with an Olympus VS200 slide scanner and processed and analysed using ImageJ2 v.2.14.0/1.5 f.

Lung histology sections were assessed for TLS by a researcher blinded to groupings and given a score between 0 and 5 based on the pathology.

Data and statistical analyses

Statistical analysis was performed using GraphPad Prism v.10.0b software.

Bulk RNA-seq data generated in this study have been deposited at the Gene Expression Omnibus (GEO) under accession number GSE243691.

Reporting summary

Further information on research design is available in the Nature Portfolio Reporting Summary linked to this article.

Data availability

All high-throughput data in this study were deposited at Gene Expression Omnibus under accession no. GSE243691 Source data are provided with this paper.

56. Schlenner, S. M. et al. Fate mapping reveals separate origins of T cells and myeloid lineages in the thymus. *Immunity* **32**, 426–436 (2010).
57. Oliphant, C. J. et al. MHCII-mediated dialog between group 2 innate lymphoid cells and CD4(+) T cells potentiates type 2 immunity and promotes parasitic helminth expulsion. *Immunity* **41**, 283–295 (2014).
58. Townsend, M. J., Fallon, P. G., Matthews, D. J., Jolin, H. E. & McKenzie, A. N. T1/ST2-deficient mice demonstrate the importance of T1/ST2 in developing primary T helper cell type 2 responses. *J. Exp. Med.* **191**, 1069–1076 (2000).
59. Puttur, F. et al. Absence of Siglec-H in MCMV infection elevates interferon alpha production but does not enhance viral clearance. *PLoS Pathog.* **9**, e1003648 (2013).
60. Nishino, K. et al. Isolation and characterisation of lymphatic endothelial cells from lung tissues affected by lymphangioleiomyomatosis. *Sci. Rep.* **11**, 8406 (2021).
61. Shao, X. et al. CellTalkDB: a manually curated database of ligand-receptor interactions in humans and mice. *Brief. Bioinform.* https://doi.org/10.1093/bib/bbaa269 (2021).

Acknowledgements We thank the Ares staff, genotyping facility and flow cytometry core for their technical assistance. We thank H.-R. Rodewald for the *Il7ra*-Cre mice. We also thank A. J. Easton (University of Warwick) for providing the PVM stock. This work was supported by the Medical Research Council as part of United Kingdom Research and Innovation (also known as UK Research and Innovation; MRC grant no. U105178805). This study was also supported by the Wellcome Trust (nos. 100963/Z/13/Z and 220223/Z/20/Z). M.K. was supported by a Gates Trust award. N.R.R. received grant funding from the European Union's Horizon 2020 research and innovation programme under Marie Skłodowska-Curie grant agreement no. 896454. J.E.M. received funding from the Rosetrees Trust. For the purpose of open access, the MRC Laboratory of Molecular Biology has applied a CC BY public copyright licence to any Author Accepted Manuscript version arising.

Author contributions M.G. designed and performed experiments and wrote the paper. P.A.C., A.C.F.F., N.R.R., M.H., M.K., J.E.M., V.C., S.-L.L. and H.E.J. performed experiments, provided advice on experimental design and interpretation and commented on the manuscript. A.N.J.M. supervised the project, designed the experiments and wrote the paper.

Competing interests A.N.J.M. is on the scientific advisory board of SinoMab. The other authors declare no competing interests.

Additional information

Supplementary information The online version contains supplementary material available at https://doi.org/10.1038/s41586-024-07746-w.

Correspondence and requests for materials should be addressed to Mayuri Gogoi or Andrew N. J. McKenzie.

Peer review information *Nature* thanks Gerard Eberl, Shigeo Koyasu and Andrew Luster for their contribution to the peer review of this work.

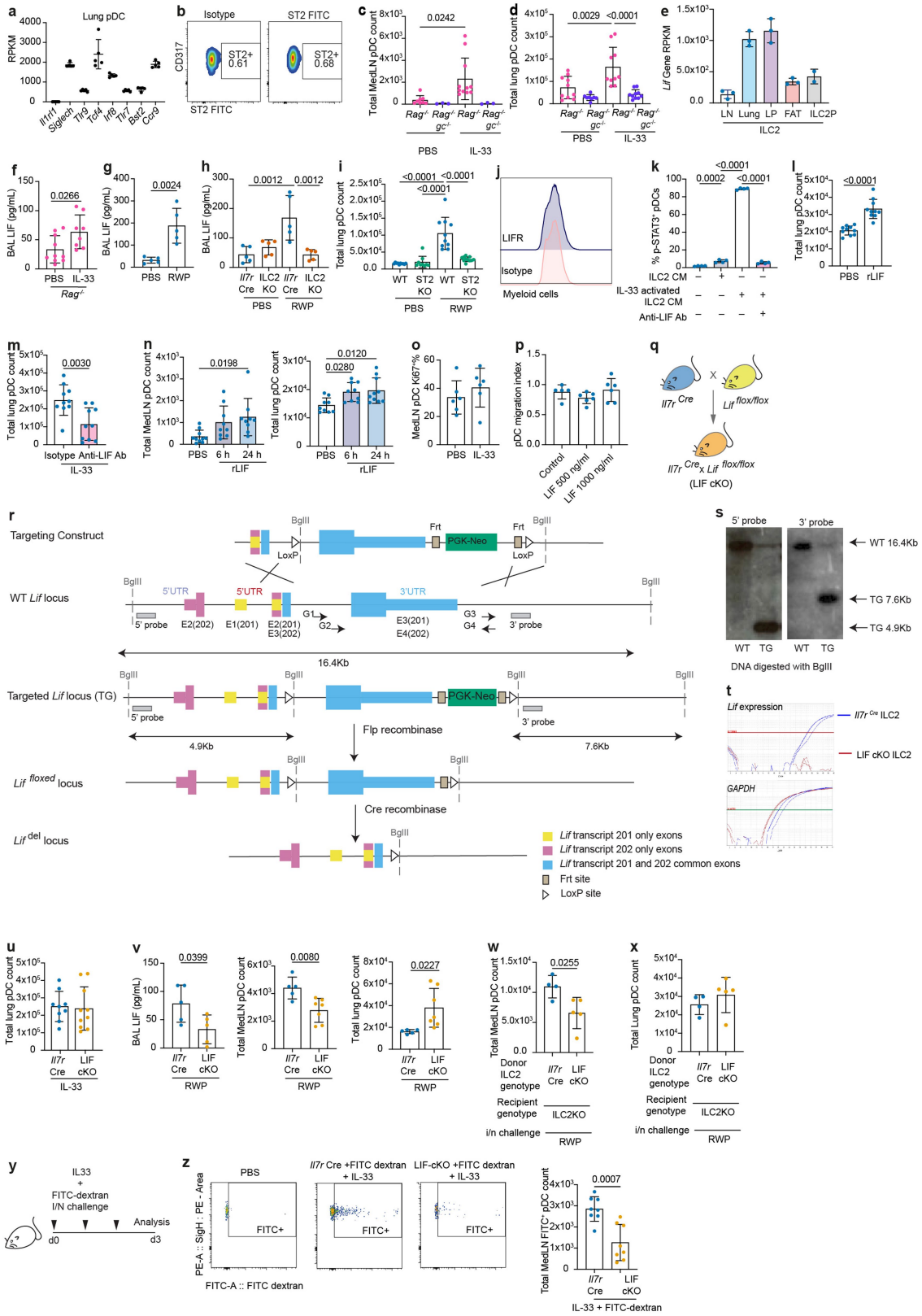

Extended Data Fig. 1 | See next page for caption.

Extended Data Fig. 1 | ILC2 production of LIF during type-2 immune response. a, Gene expression of indicated genes in pDCs from bulk RNAseq data with five biological replicates per group. **b**. Representative flow cytometry plots of lung pDCs stained for ST2. Flow cytometry analysis of pDC numbers in **c**, MedLN, *Rag2*$^{-/-}$ (PBS = 8, IL-33 = 11) and *Rag2*$^{-/-}$*Il2rgc*$^{-/-}$ (*Rag2*$^{-/-}$*gc*$^{-/-}$) (PBS = 3, IL-33 = 3), and **d**, lung *Rag2*$^{-/-}$ (PBS = 10, IL-33 = 10) and *Rag2*$^{-/-}$*gc*$^{-/-}$ (PBS = 8, IL-33 = 10) following IL-33 intranasal challenge. **e**, *Lif* expression in ILC2 purified from lymph node (LN) (n = 3), lung (Lung) (n = 3), small intestine lamina propria (LP) (n = 3), adipose tissue (FAT) (n = 3), bone marrow ILC2 progenitor (ILC2P) (n = 2) from naïve mice. ELISA of LIF in the BAL **f**, from *Rag2*$^{-/-}$ (PBS = 10, IL-33 = 8) mice following IL-33 intranasal challenge, and **g**, from wildtype mice (WT) following ragweed protein extract (RWP) challenge (PBS = 5, RWP = 5), and from **h**, *Il7r*^{Cre} (PBS = 5, RWP = 5) and *Il7r*^{Cre} x *Rora*$^{flox/flox}$ (ILC2KO) (PBS = 5, RWP = 5) mice treated with RWP. **i**, Flow cytometry analysis of lung pDCs in WT (PBS = 10, RWP = 10 IL-33 receptor-deficient (ST2KO) (PBS = 9, RWP = 11) mice following RWP intranasal challenge. **j**, Flow cytometry analysis of LIF receptor (LIFR) staining on lung myeloid cells. Flow cytometry analysis of **k**, phospho-STAT3 positive cells following activation as indicated, ILC2 conditioned media (ILC2 CM), IL-33 activated ILC2 conditioned media (IL-33 activated ILC2 CM), anti-LIF neutralizing antibody (n = 4), and **l**, lung pDCs following rLIF treatment in wildtype mice (n = 10), and **m**, lung pDCs in wild type mice following treatment with anti-LIF neutralizing antibody or isotype and IL-33 intranasal challenge (n = 10), and **n**, pDCs in the MedLN (PBS = 10, 6 h = 9, 24 h = 9) and lung (PBS = 9, 6 h = 9, 24 h = 10) at the indicated timepoints following one dose of rLIF challenge, and **o**, MedLN pDC Ki67 expression in wild type mice following IL-33 challenge (n = 6). **p**, Trans-well chemotaxis of pDCs to rLIF. (control = 5, LIF (500 ng/ml) = 6, LIF (1000 ng/ml) = 6). **q**, *Il7r*^{Cre} x *Lif*$^{flox/flox}$ (LIF-cKO) generation schematic. **r**, Schematic of *Lif*$^{flox/flox}$ mouse generation. **s**, Southern analysis of *Lif*$^{flox/flox}$ ES cells. **t**, qPCR analysis of *Lif* expression in ILC2s purified from *Il7r*^{Cre} and *Il7r*^{Cre} x *Lif*$^{flox/flox}$ (LIF-cKO) mice. **u**, Flow cytometry analysis of lung pDC numbers in *Il7r*^{Cre} (n = 9) and LIF-cKO (n = 10) following IL-33 challenge. **v**, ELISA of BAL LIF from RWP challenged *Il7r*^{Cre} and LIF-cKO mice (*Il7r*^{Cre} = 5 and LIF-cKO =5), and flow cytometry analysis of MedLN pDCs (*Il7r*^{Cre} = 5 and LIF-cKO =7) and lung pDCs (*Il7r*^{Cre} = 5 and LIF-cKO =7). Flow cytometry analysis of **w**, MedLN, and **x**, lung pDCs in recipient ILC2 KO mice transplanted with *Il7r*^{Cre} or LIF-cKO ILC2s and subsequently challenged with RWP. (*Il7r*^{Cre} = 4 and LIF-cKO =5). **y**, Schematic of mouse FITC-dextran and IL-33 intranasal challenge. **z**, Flow cytometry gating strategy and MedLN FITC-dextran^{+} pDCs numbers in *Il7r*^{Cre} and LIF-cKO mice following PVM and FITC-dextran intranasal challenge (*Il7r*^{Cre} = 8 and LIF-cKO =8). **f-h,m-p,u-x,z**, unpaired two-sided *t*-test, **c,d,i,k,l** one-way ANOVA with Tukey's multiple comparisons test. Data mean ± SEM. Data are representative of two (b, g, h, j, k, o, p, v, w, x) independent experiments with similar results. Experiments in (c, d, f, i, l, m, n, u, z) are pooled data from two independent experiments. RNA-seq data in a are based on five biological replicates per group.

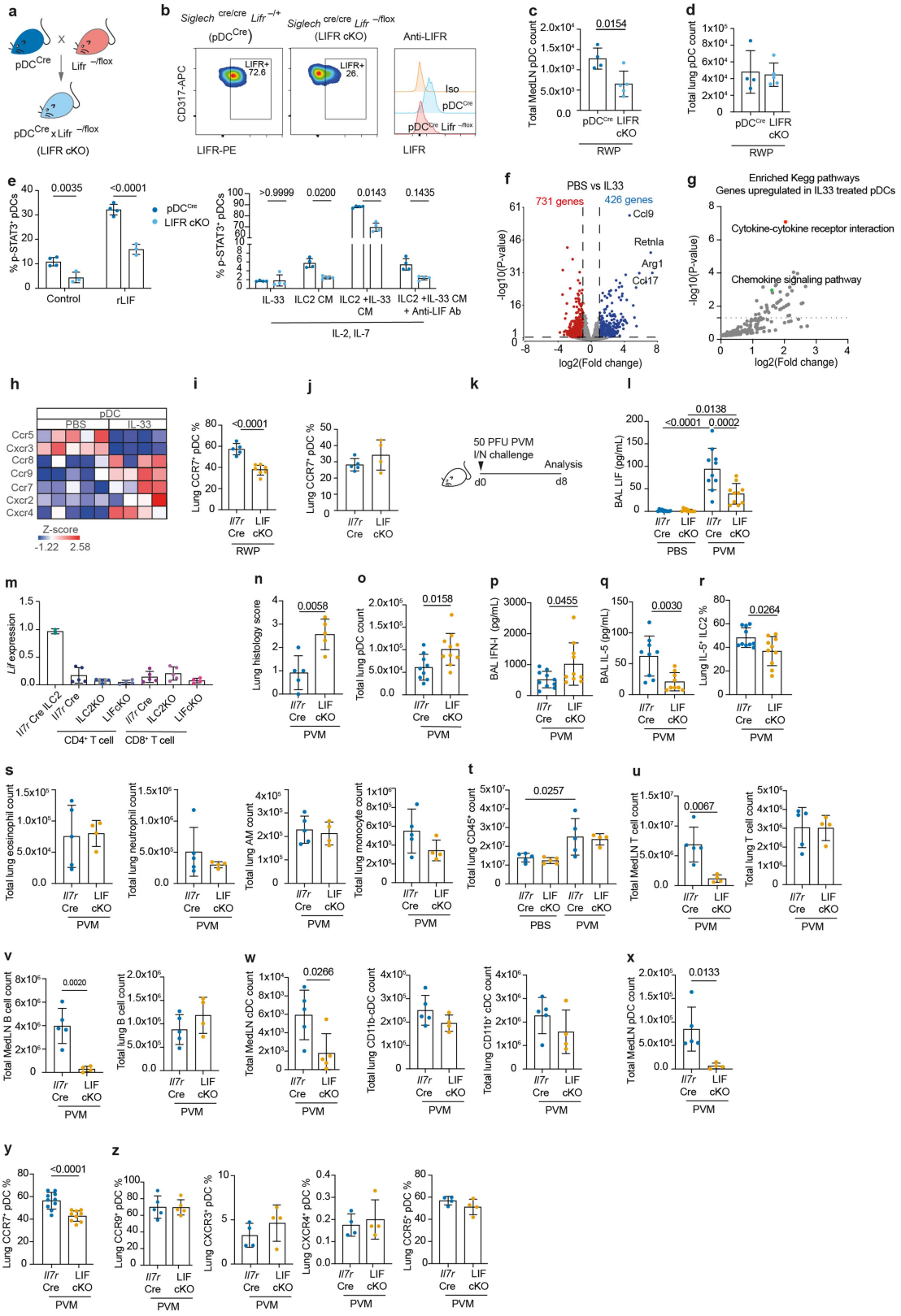

Extended Data Fig. 2 | See next page for caption.

Extended Data Fig. 2 | pDC expression of LIFR and Pneumovirus infection of conditional LIF-deficient mice. a, Schematic of pDC-specific LIF receptor (LIFR) deficient pDC^{Cre} x *Lifr* $^{-/flox}$ (LIFR cKO) mice generation. **b**, LIF receptor (LIFR) expression in lung pDCs in *Siglech* $^{Cre/Cre}$ x *Lifr* $^{-/+}$ (pDC^{Cre}) and *Siglech* $^{Cre/Cre}$ x *Lifr* $^{-/flox}$ (LIFR cKO) mice. Flow cytometry analysis of pDC^{Cre} and LIFR cKO **c**, MedLN, and **d**, lung pDCs following RWP challenge (pDC^{Cre} =4 and LIFR cKO = 5). **e**, Flow cytometry analysis of phospho-STAT3 positive cells following activation as indicated, ILC2 conditioned media (ILC2 CM), IL-33 activated ILC2 conditioned media (IL-33 + ILC2 CM), anti-LIF neutralizing antibody (control pDC^{Cre} = 4, control LIFR cKO =3, rLIF pDC^{Cre} = 4, rLIF LIFR cKO =3, IL-33 = 4, ILC2 CM = 4, IL-33 + ILC2 CM = 4, IL-33 + ILC2 CM+Anti-LIF Ab =4). **f**, Volcano plot of all differentially expressed genes in bulk RNAseq of lung pDCs from PBS or IL-33 challenged wildtype mice. **g**, KEGG pathway analysis of significant differentially expressed genes from (**f**). **h**, Heatmap of significant differentially expressed chemokine receptor genes from lung pDC bulk RNAseq. Flow cytometry analysis of lung **i**, $CCR7^+$ pDCs in LIF-cKO mice after RWP challenge (*Il7r* ^{Cre} = 5 and LIF-cKO =7), and **j**, $CCR7^+$ pDCs in naïve LIF-cKO mice (*Il7r* ^{Cre} = 5 and LIF-cKO =4). **k**, schematic of the experimental protocol for pneumovirus of mouse (PVM) infection. **l**, ELISA of LIF in the BAL from *Il7r* ^{Cre} and LIF-cKO mice following PVM challenge (n = 10). **m**, qPCR analysis of *Lif* gene expression in ILC2s, $CD4^+$ and $CD8^+$ T cells purified from indicated mice following PVM intranasal challenge. *Il7r* ^{Cre}, ILC2KO and LIF-cKO mice (*Il7r* ^{er} ILC2 = 2, *Il7r* ^{Cre} $CD4^+$T = 5, *Il7r* ^{Cre} $CD8^+$ T = 4, ILC2KO $CD4^+$T =4, ILC2KO $CD8^+$ T = 5, LIF-cKO $CD4^+$T =4, LIF-cKO $CD8^+$ T = 5). **n**, Lung histology infiltration score of *Il7r* ^{Cre} and LIF-cKO mice following PVM challenge (*Il7r* ^{Cre} = 5 and LIF-cKO =5). **o**, Flow cytometry analysis of lung pDCs in *Il7r* ^{Cre} and LIF-cKO mice following PVM challenge (*Il7r* ^{Cre} = 9 and LIF-cKO =10). ELISA of: **p**, IFN-I in BAL (*Il7r* ^{Cre} = 10 and LIF-cKO =10);and **q**, IL-5 in BAL (*Il7r* ^{Cre} = 9 and LIF-cKO =9) from *Il7r* ^{Cre} and LIF-cKO mice following PVM challenge. **r**, Flow cytometry analysis of lung IL-5^+ILC2s in lung in *Il7r* ^{Cre} and LIF-cKO mice after PVM challenge (*Il7r* ^{Cre} = 10 and LIF-cKO =10). **s**, Flow cytometry analysis of MedLN and lung eosinophil, neutrophil, alveolar macrophage (AM) and monocyte numbers following PVM challenge (*Il7r* ^{Cre} = 5 and LIF-cKO =4). Flow cytometry analysis of **t**, lung $CD45^+$ cell numbers *Il7r* ^{Cre} (PBS = 5, PVM = 5) and LIF-cKO (PBS = 5, PVM = 4); **u**, T cell numbers; **v**, B cells; **w**, cDC; **x**, pDCs from MedLN and lung from *Il7r* ^{Cre} and LIF-cKO mice following PVM challenge (*Il7r* ^{Cre} = 5 and LIF-cKO =4). **y**, Flow cytometry analysis of lung pDCs for CCR7 expression in *Il7r* ^{Cre} and LIF-cKO mice following PVM challenge (*Il7r* ^{Cre} = 10 and LIF-cKO =11). **z**, Flow cytometry analysis of lung pDCs for CCR9 (*Il7r* ^{Cre} = 5 and LIF-cKO =5), CXCR3 (*Il7r* ^{Cre} = 4 and LIF-cKO =4), CXCR4 (*Il7r* ^{Cre} = 4 and LIF-cKO =4), and CCR5 (*Il7r* ^{Cre} = 4 and LIF-cKO =4) in *Il7r* ^{Cre} and LIF-cKO mice following PVM challenge. **c,d,i,j,n-s,u-z** unpaired two-sided *t*-test, **e,l,t** one-way ANOVA with Tukey's multiple comparisons test. Data mean ± SEM. Data are representative of two (b, c, d, e, l, i,j,m,n,s-x,z) independent experiments with similar results. Experiments in (l,o-r,y) are pooled data from two independent experiments. RNA-seq data in a are based on five biological replicates per group.

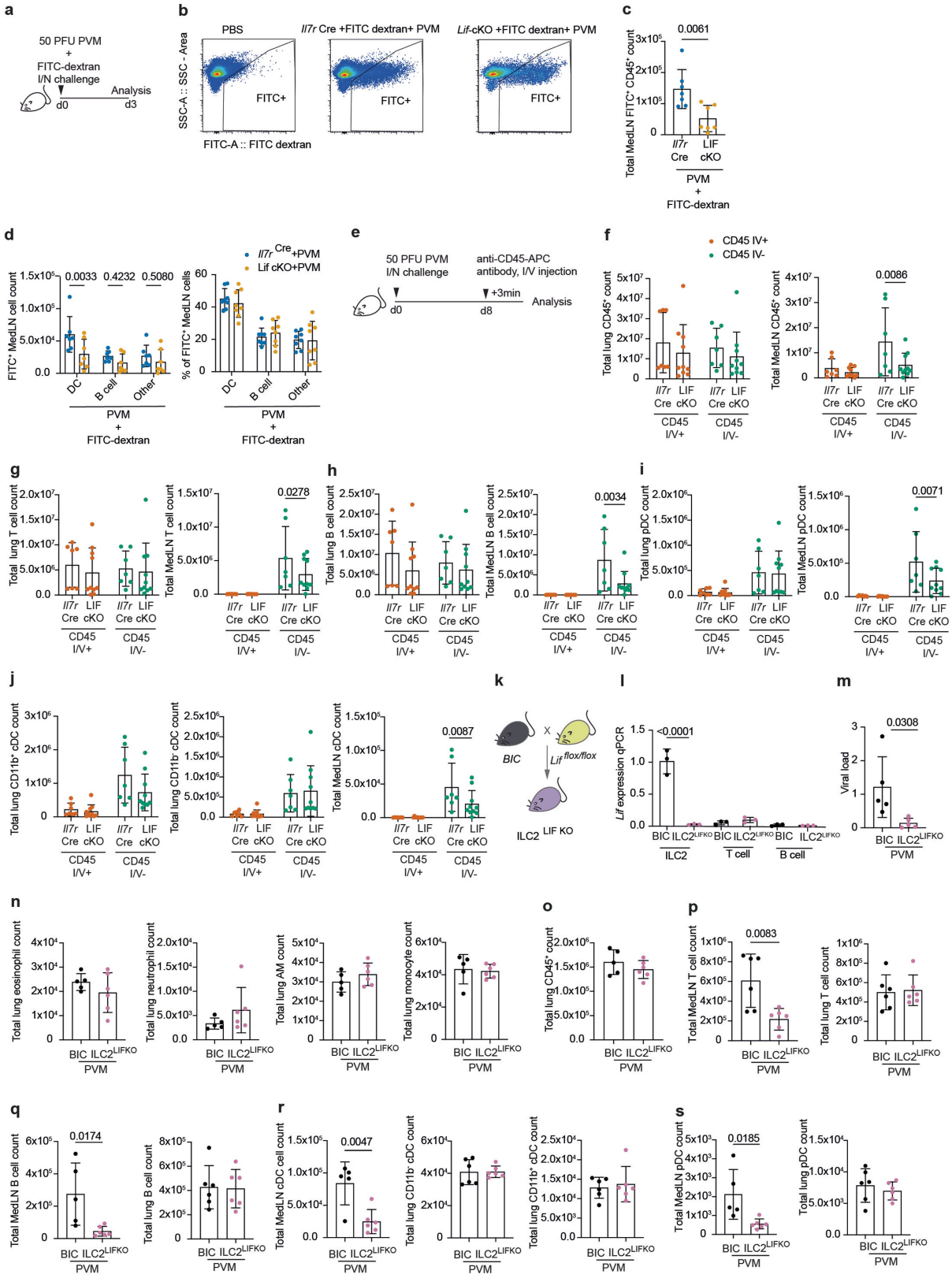

Extended Data Fig. 3 | See next page for caption.

Extended Data Fig. 3 | Assessment of circulating and tissue-resident immune cells in conditional LIF-deficient mice during PVM infection. **a**, Schematic of FITC-dextran and PVM intranasal challenge. **b**, Flow cytometry gating strategy and FITC-dextran$^+$ CD45$^+$ MedLN cell numbers in *Il7r*^{Cre} and LIF-cKO mice following PVM and FITC-dextran intranasal challenge. Flow cytometry analysis of: **c**, MedLN FITC-dextran$^+$ cell numbers in *Il7r*^{Cre} and LIF-cKO mice following PVM and FITC-dextran intranasal challenge (*Il7r*^{Cre} = 7 and LIF-cKO =7); **d**, MedLN FITC-dextran$^+$ DCs, B cells, and other immune cell numbers (*Il7r*^{Cre} = 7 and LIF-cKO =7) and percentages in *Il7r*^{Cre} and LIF-cKO mice following PVM and FITC-dextran intranasal challenge (*Il7r*^{Cre} = 8 and LIF-cKO =8). **e**, Schematic of intravenous anti-CD45-APC antibody labelling after PVM infection. Flow cytometry analysis of lung and MedLN intravenous anti-CD45-APC antibody labelled: **f**, CD45$^+$ immune cells, **g**, T cells, **h**, B cells, **i**, pDCs, and **j**, cDCs after PVM infection (*Il7r*^{Cre} = 7 and LIF-cKO =10). **k**, ILC2^{LIFKO} generation schematic. **l**, qPCR analysis of *Lif* expression in lung ILC2, T cells and B cells purified from Boolean Cre (BIC) and BIC x *Lif*$^{flox/flox}$ (ILC2^{LIFKO}) mice after PVM challenge (BIC = 3, ILC2^{LIFKO} = 3). **m**, Lung viral load BIC and ILC2^{LIFKO} mice following PVM challenge (BIC = 5, ILC2^{LIFKO} = 5). **n**, Flow cytometry analysis of lung eosinophil (BIC = 5, ILC2^{LIFKO} = 5), neutrophils (BIC = 5, ILC2^{LIFKO} = 6), alveolar macrophages (AM) (BIC = 5, ILC2^{LIFKO} = 6) and monocytes (BIC = 5, ILC2^{LIFKO} = 6) in BIC and ILC2^{LIFKO} mice following PVM intranasal challenge. Flow cytometry analysis of: **o**, lung CD45$^+$ cells (BIC = 5, ILC2^{LIFKO} = 6); **p**, T cells from MedLN (BIC = 6, ILC2^{LIFKO} = 6) and lung (BIC = 6, ILC2^{LIFKO} = 6); **q**, B cells from MedLN (BIC = 5, ILC2^{LIFKO} = 6) and lung (BIC = 6, ILC2^{LIFKO} = 6); **r**, cDCs from MedLN (BIC = 5, ILC2^{LIFKO} = 6) and lung (BIC = 6, ILC2^{LIFKO} = 6); **s**, pDCs from MedLN (BIC = 5, ILC2^{LIFKO} = 6) and lung (BIC = 6, ILC2^{LIFKO} = 6). **c,d,f-j,l-s** unpaired two-sided *t*-test. Data mean ± SEM. Data are representative of two (**b, l,m-s**) independent experiments with similar results. **c,d,f-j** unpaired two-sided *t*-test. Data mean ± SEM. Data are pooled from two independent experiments.

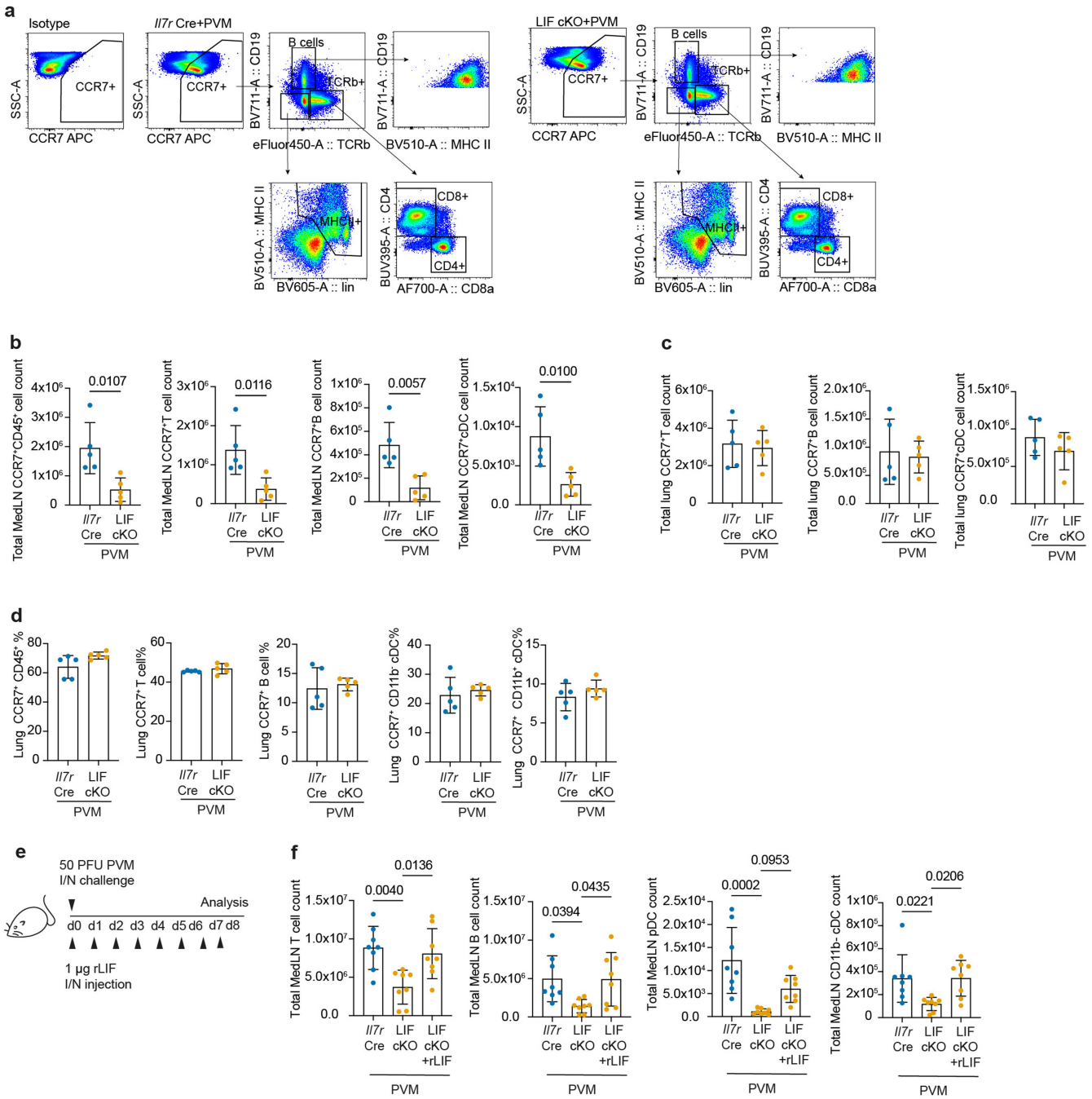

Extended Data Fig. 4 | CCR7-positive immune cell analysis in conditional LIF-deficient mice. a, Flow cytometry gating strategy for CCR7$^+$ CD45$^+$ cells in *Il7r*^{Cre} and LIF-cKO mice following PVM challenge. **b-d**, *Il7r*^{Cre} and LIF-cKO mice following PVM challenge (*Il7r*^{Cre} = 5 and LIF-cKO = 5). **b**, Flow cytometry analysis of CCR7$^+$ cell numbers in MedLN; **c**, Flow cytometry analysis of CCR7$^+$ cell numbers in lung. **d**, Flow cytometry analysis of CCR7$^+$ cell percentages. **e**, Schematic of PVM infection combined with PBS or rLIF intranasal treatment. **f**, Flow cytometry analysis of MedLN T cells, B cells, pDCs and cDCs in *Il7r*^{Cre} and LIF-cKO mice treated with rLIF and infected with PVM (*Il7r*^{Cre} = 8 and LIF-cKO = 8). **b-d**, unpaired two-sided *t*-test, **f**, one-way ANOVA with Tukey's multiple comparisons test. Data mean ± SEM. Data are representative of two (a, b, c, d) independent experiments with similar results. Experiment (f) are pooled data from two independent experiments.

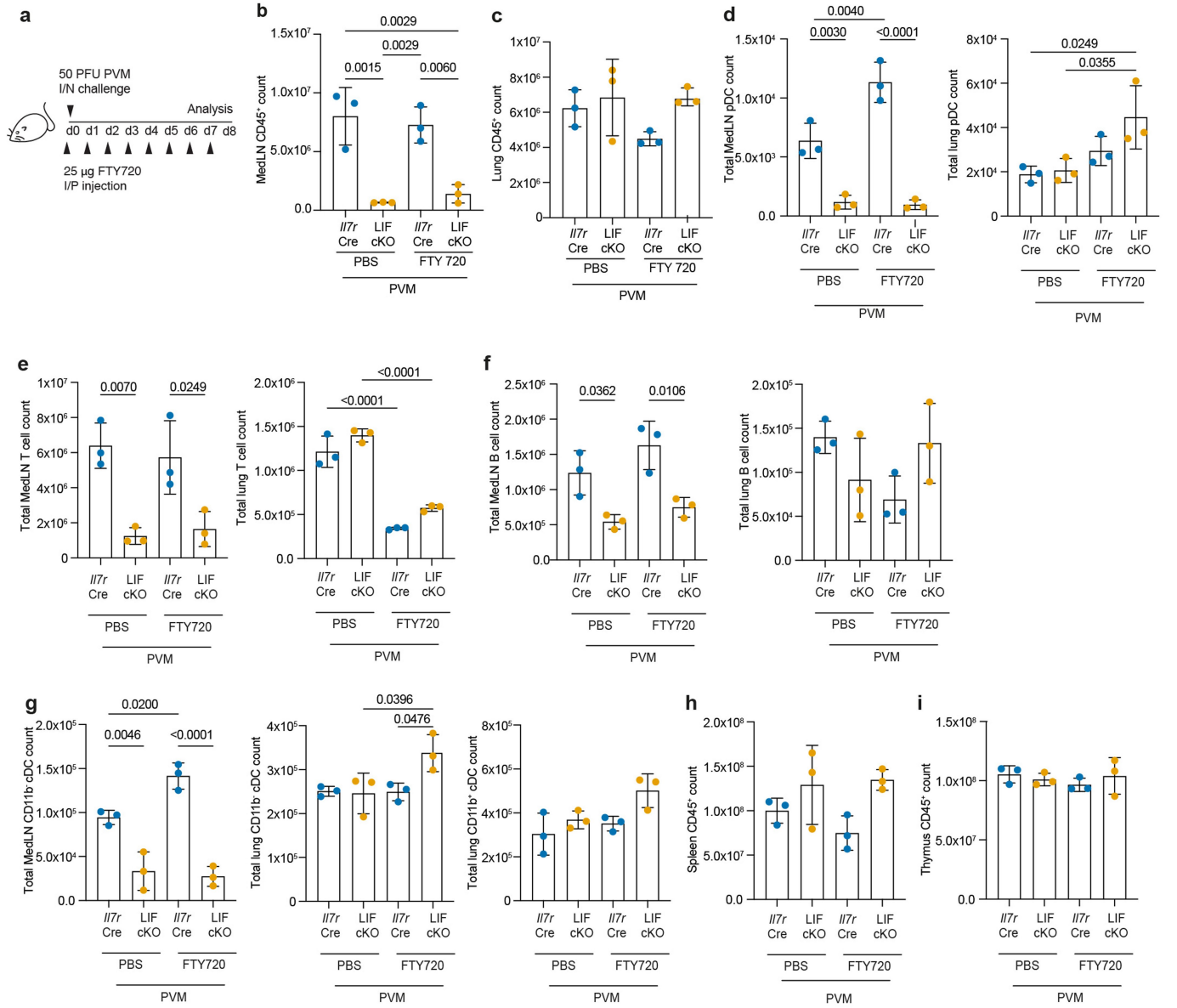

Extended Data Fig. 5 | FTY720 treatment of conditional LIF-deficient mice. **a**, Schematic of PVM intranasal infection with PBS or FTY720 treatment. Flow cytometry analysis of **b**, MedLN CD45$^+$ cells; **c**, lung CD45$^+$ cells; **d**, MedLN and lung pDCs; **e**, MedLN and lung T cells; **f**, MedLN and lung B cells; **g**, MedLN and lung cDCs; **h**, spleen CD45$^+$ cells; and **i**, thymus CD45$^+$ cells in *Il7r*^{Cre} and LIF-cKO mice treated with PBS or FTY720 following PVM challenge. (n = 3). **b-i**, one-way ANOVA with Tukey's multiple comparisons test. Data mean ± SEM. Data are representative of two (b-i) independent experiments with similar results.

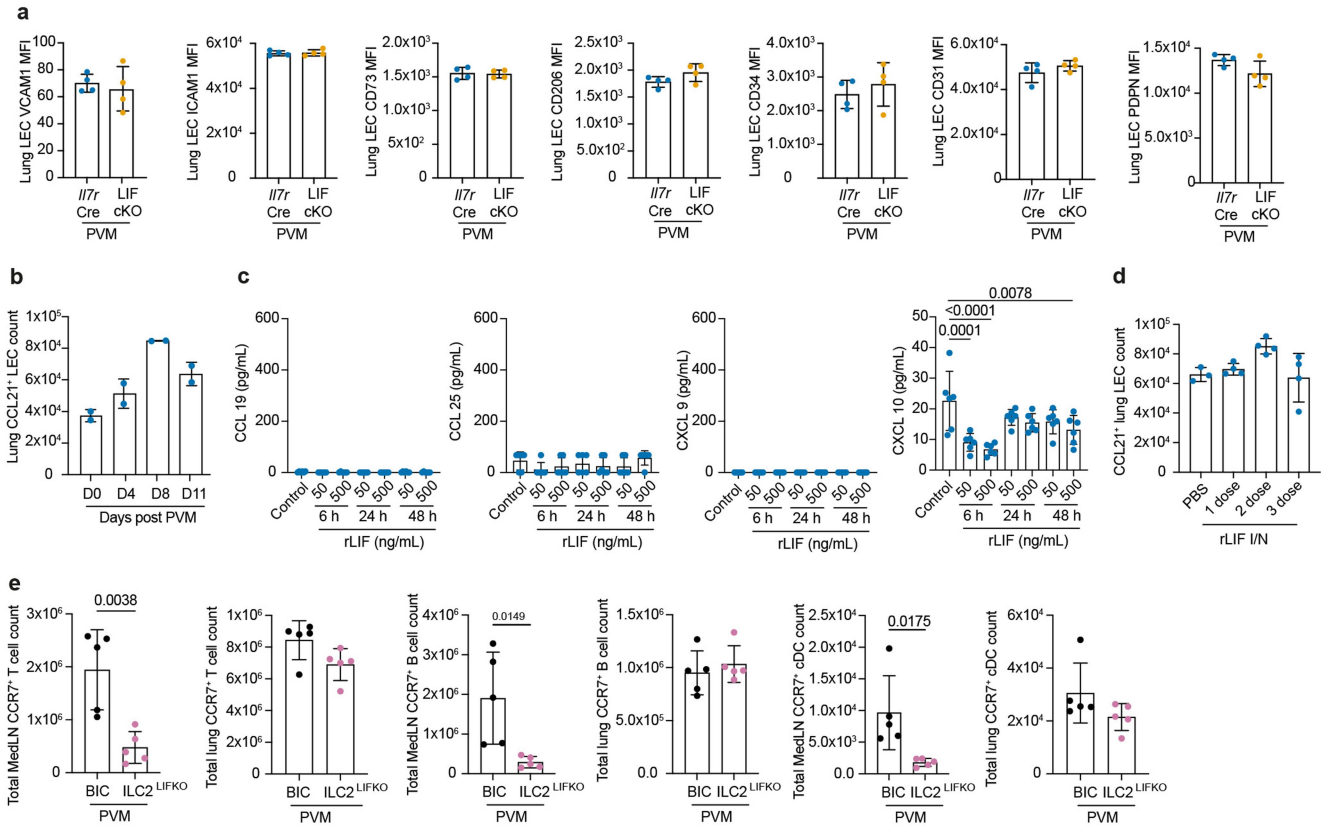

Extended Data Fig. 6 | Adhesion molecule and chemokine receptor expression by lung LECs. Flow cytometry analysis of: **a**, lung LEC for adhesion molecules VCAM1, ICAM1, CD73, CD206, CD34, CD31, Podoplanin (PDPN) from *Il7r*^{Cre} and LIF-cKO mice following PVM challenge (n = 4), **b**, CCL21^{+} lung LEC numbers in wildtype mice following PVM challenge at indicated timepoints (n = 2). **c**, ELISA of CCL19, CCL25, CXCL9, CXCL10 concentration in in-vitro cultured LEC conditioned media following rLIF treatment for 6 h or 24 h or 48 h (n = 6). **d**, Flow cytometry analysis of CCL21^{+} lung LEC numbers in wildtype mice following rLIF challenge at indicated timepoint (PBS = 3, rLIF =4). **e**, Flow cytometry analysis of MedLN and lung CCR7^{+} T cells, CCR7^{+} B cells, and CCR7^{+} cDCs from BIC and ILC2^{LIFKO} mice following PVM challenge (n = 5). **a,d,e**, unpaired two-sided *t*-test, **c**, one-way ANOVA with Tukey's multiple comparisons test. Data mean ± SEM. Data are representative of two (a, b, d, e) independent experiments with similar results. Experiments in (c) are pooled data from two independent experiments.

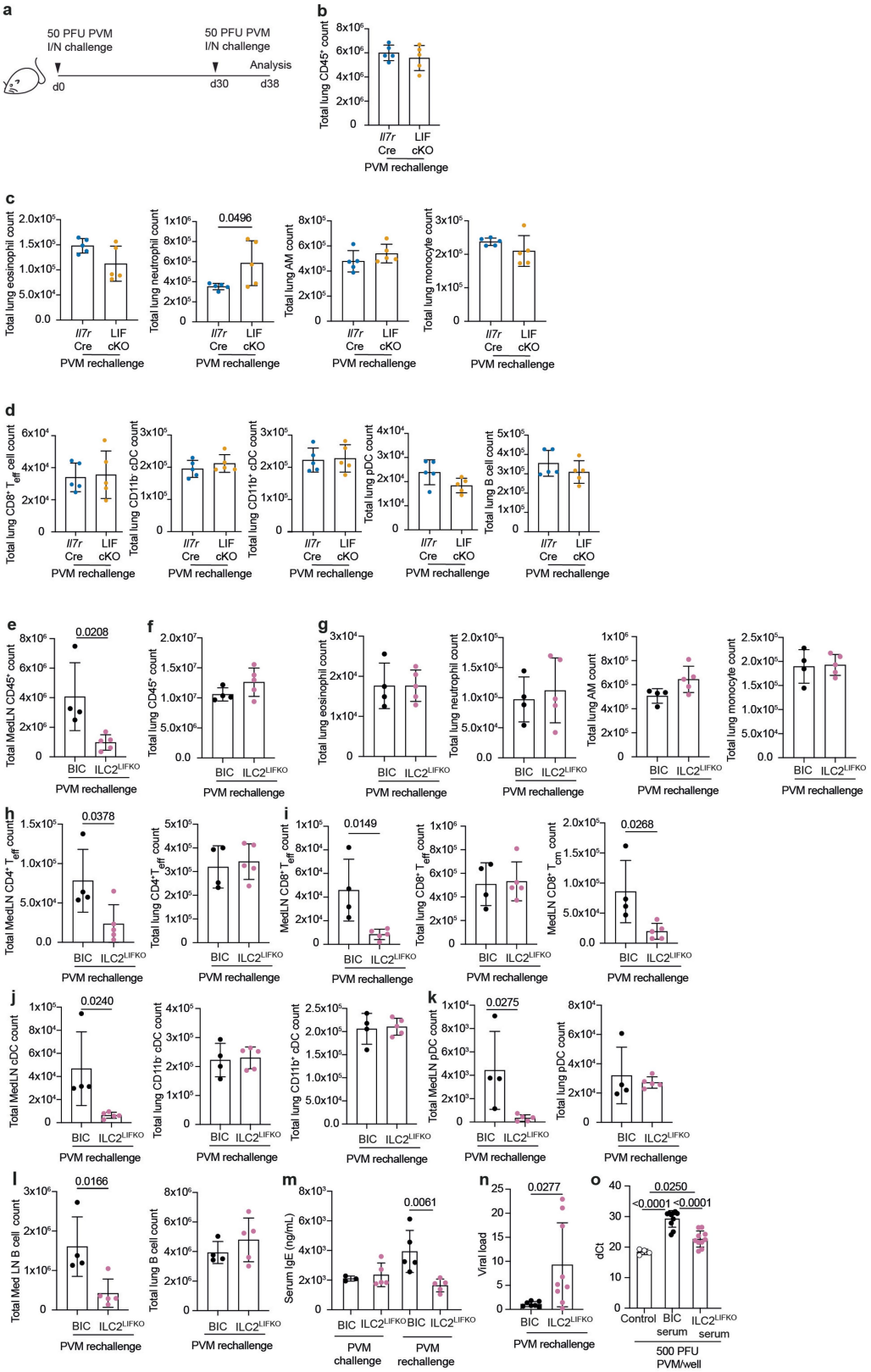

Extended Data Fig. 7 | See next page for caption.

Extended Data Fig. 7 | Pneumovirus reinfection in conditional LIF-deficient mice. a, Schematic of PVM intranasal primary and secondary infection. Flow cytometry analysis of lung: **b**, $CD45^+$; **c**, eosinophil, neutrophil, alveolar macrophage (AM) and monocyte; **d**, $CD4^+T_{Eff}$ cells, $CD8^+T_{Eff}$ cells and T_{CM} cells, DCs, pDCs and B cell numbers from *Il7r*^{Cre} and LIF-cKO mice following PVM rechallenge (n = 5). Flow cytometry analysis of **e**, MedLN $CD45^+$ cells; **f**, lung $CD45^+$ cells; **g**, lung eosinophils, neutrophils, alveolar macrophages (AM) and monocytes; **h**, MedLN and lung $CD4^+$ T_{Eff} cells; **i**, MedLN and lung $CD8^+$ T_{Eff} and $CD8^+$ T_{CM} cells; **j**, MedLN and lung cDCs; **k**, MedLN and lung pDCs, and **l**, MedLN and lung B cells in BIC and $ILC2^{LIFKO}$ mice following PVM rechallenge (BIC = 4 and $ILC2^{LIFKO}$ = 5). **m**, ELISA of serum IgE from BIC and $ILC2^{LIFKO}$ mice following PVM primary and secondary challenge (PVM challenged BIC = 3, PVM challenged $ILC2^{LIFKO}$ = 5, PVM rechallenged BIC = 5, PVM rechallenged $ILC2^{LIFKO}$ = 5;). **n**, Lung viral load in BIC and $ILC2^{LIFKO}$ mice following PVM rechallenge (BIC = 7 and $ILC2^{LIFKO}$ = 9). **o**, In vitro viral neutralization assay with BIC and $ILC2^{LIFKO}$ mice serum following PVM rechallenge. dC_T was calculated as C_T(PVM)-C_T(hamster GAPDH) (control = 4, PVM rechallenged BIC serum =10 and PVM rechallenged $ILC2^{LIFKO}$ serum =10). **b-o**, unpaired two-sided *t*-test. Data mean ± SEM. Data are representative of two (b-m) independent experiments with similar results. Experiments in (n,o) are pooled data from two independent experiments.

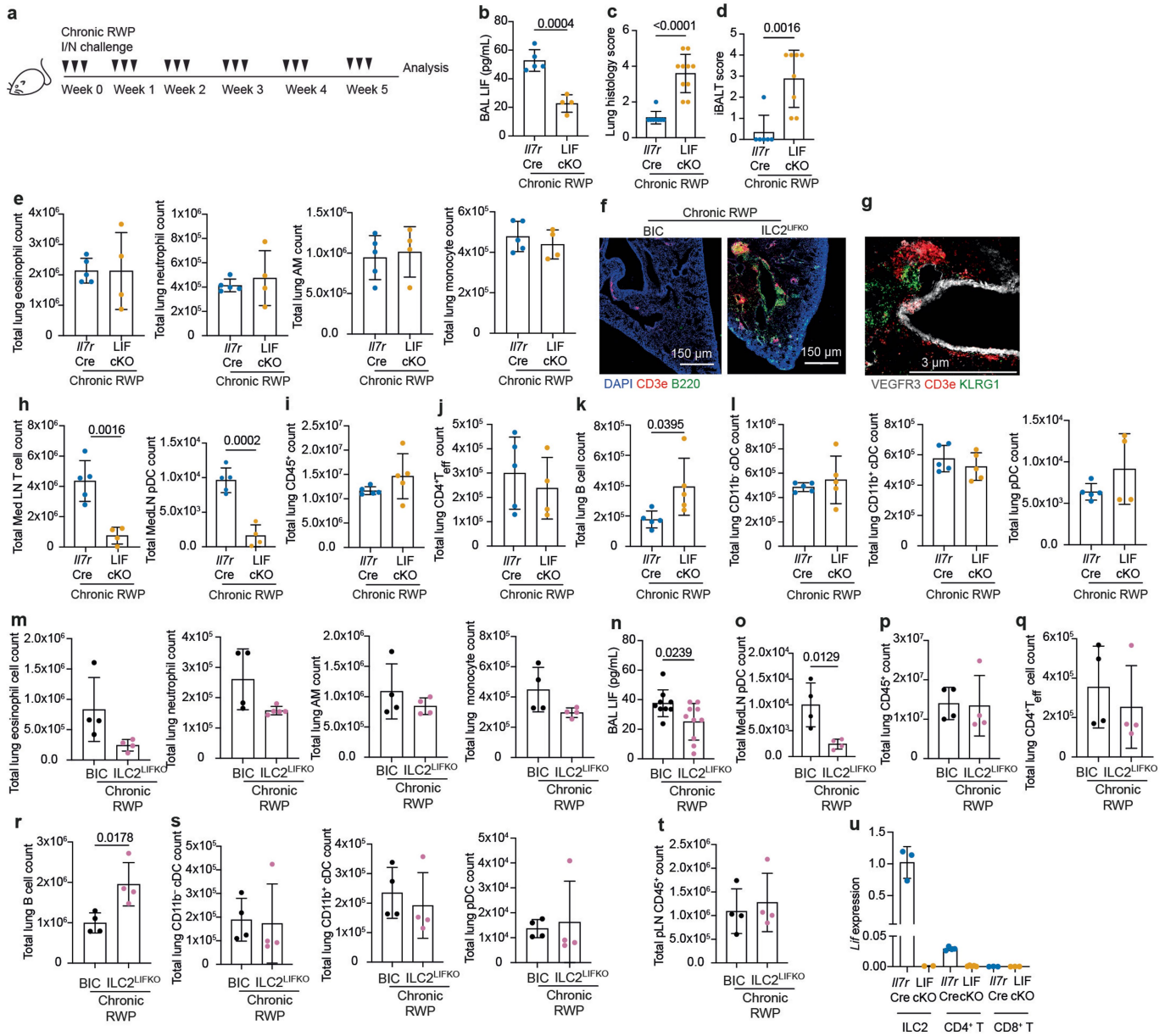

Extended Data Fig. 8 | Chronic RWP challenge of conditional LIF-deficient mice. a, Schematic of chronic RWP intranasal challenge protocol. **b**, ELISA of LIF in BAL from *Il7r*^{Cre} and LIF-cKO mice following chronic RWP challenge (*Il7r*^{Cre} = 5, LIF-cKO =4). **c**, Lung histology scores from *Il7r*^{Cre} and LIF-cKO mice following chronic RWP challenge (*Il7r*^{Cre} = 8, LIF-cKO =10). **d**, Lung iBALT scores from *Il7r*^{Cre} and LIF-cKO mice following chronic RWP challenge. (*Il7r*^{Cre} = 6, LIF-cKO =8). **e**, Flow cytometry analysis of lung eosinophils, neutrophils, alveolar macrophages and monocytes in *Il7r*^{Cre} and LIF-cKO mice following chronic RWP challenge (*Il7r*^{Cre} = 5, LIF-cKO =4). **f**, Immunofluorescence histology of lung showing tertiary lymphoid tissue formation in BIC and ILC2^{LIFKO} mice following chronic RWP challenge, B cells stained with B220 antibody (green), T cells with CD3e antibody (red) and nuclei with DAPI (blue). **g**, Immunofluorescence histology of lung from LIF-cKO mouse after chronic RWP intranasal challenge. KLRG1 (green), CD3e (red) and VEGFR3 (grey). Flow cytometry analysis of **h**, MedLN T cells and pDCs (*Il7r*^{Cre} = 5, LIF-cKO =4); **i**, lung CD45$^+$ cells (*Il7r*^{Cre} = 5, LIF-cKO =5), **j**, lung CD4$^+$ T$_{Eff}$ cells (*Il7r*^{Cre} = 5, LIF-cKO =4), **k**, lung B cells (*Il7r*^{Cre} = 5, LIF-cKO =5), **l**, lung cDCs (*Il7r*^{Cre} = 5, LIF-cKO =5) and pDCs (*Il7r*^{Cre} = 5, LIF-cKO =4) from *Il7r*^{Cre} and LIF-cKO mice following chronic RWP challenge. **m**, Flow cytometry analysis of lung eosinophils, neutrophils, alveolar macrophages (AM) and monocytes in Boolean Cre (BIC) and BIC x *Lif*$^{flox/flox}$ (ILC2^{LIFKO}) mice following chronic RWP challenge (n = 4). **n**, ELISA of LIF in BAL from BIC and ILC2^{LIFKO} mice following chronic RWP challenge (BIC = 9, ILC2^{LIFKO} = 10). Flow cytometry analysis of **o**, MedLN pDCs; **p**, lung CD45$^+$ cells; **q**, lung CD4$^+$ T$_{Eff}$ cells; **r**, lung B cells; **s**, lung cDCs and pDCs, and **t**, inguinal lymph node (pLN) CD45$^+$ cells in BIC and ILC2^{LIFKO} mice following chronic RWP challenge (n = 4). **u**, qPCR analysis of *Lif* expression in lung ILC2, CD4$^+$ and CD8$^+$ T cell purified from *Il7r*^{Cre} and LIF-cKO mice following chronic RWP challenge (n = 2-4). **b-e, h-t** unpaired two-sided *t*-test. Data mean ± SEM. Data are representative of two (b, e, f, g, h, i, j, k, l, m, o, p, q, r, s, t, u) independent experiments with similar results. Experiments in (c, d, n) are pooled data from two independent experiments.

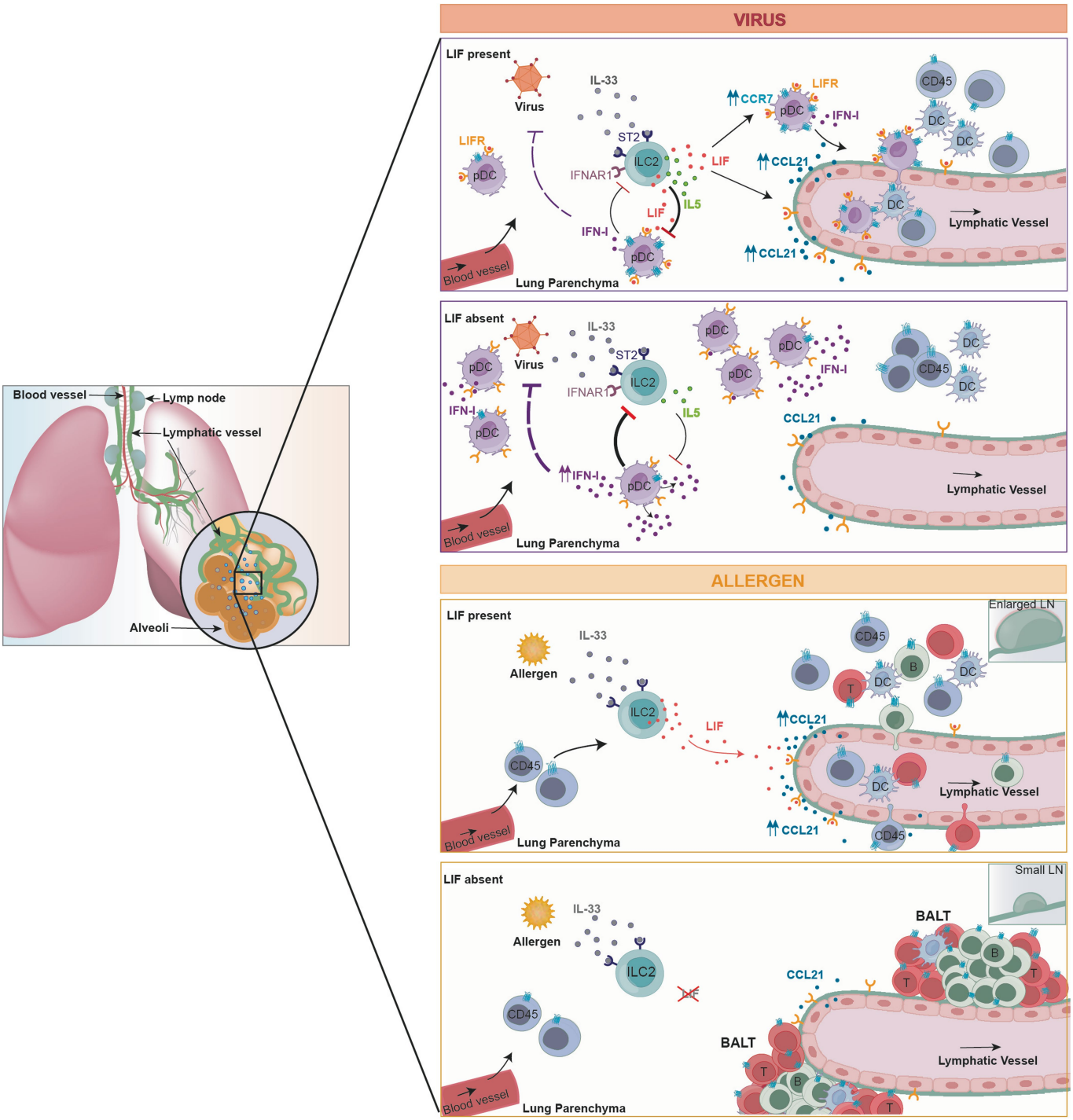

Extended Data Fig. 9 | Schematic of the roles of ILC2-derived LIF regulation of immune cell migration during pulmonary responses to viral infection and allergen challenge.

Extended Data Table 1 | Reagent list

Antibody	Fluorophore	Dilution	Clone	Catalogue number	Supplier
CD45	BUV395	1/500	30-F11	565967	BD Biosciences
CD11b	BUV395	1/500	M1/70	563553	BD Biosciences
Siglec F	AF647	1/500	E50-2440	562680	BD Biosciences
CD4	BUV395	1/500	GK1.5	563790	BD Biosciences
TCRb	BUV496	1/250	H57-597	749915	BD Biosciences
CD11b	BUV737	1/500	M1/70	612800	BD Biosciences
CD4	BUV737	1/500	RM4-5	612844	BD Biosciences
SA BUV737	BUV737	1/300		612775	BD Biosciences
Thy1.2 (CD90.2)	BUV805	1/500	BD	741909	BD Biosciences
CD11b	BV750	1/300	M1/70	746910	BD Biosciences
ICAM1	AF647	1/500	YN1/1.7.4	116114	Biolegend
CD19	AF700	1/500	6D5	115528	Biolegend
CD8a	AF700	1/500	53-6.7	100730	Biolegend
FcεRIα	AF700	1/500	MAR-1	134324	BioLegend
TNF	AF700	1/300	MP6-XT22	506338	Biolegend
IL5	APC	1/300	TRFK5	504306	BioLegend
CD11b	Biotin	1/500	M1/70	101204	Biolegend
CD127	Biotin	1/500	SB/199	121104	Biolegend
CD317	Biotin	1/500	927	127006	Biolegend
CD4	Biotin	1/500	GK1.5	100404	Biolegend
TCRb	Biotin	1/500	H57-597	109204	Biolegend
NK1.1	BUV395	1/500	PK136	564144	BD Biosciences
Cd11c	BV421	1/500	N418	117330	Biolegend
Gr1	BV421	1/300	RB6-8C5	108433	Biolegend
NK1.1	BV421	1/500	PK136	108731	BioLegend
SA BV421	BV421	1/300		405225	Biolegend
CD25	BV510	1/300	PC61	102042	Biolegend
CD45	BV510	1/500	30-F11	103138	Biolegend
IA/IE	BV510	1/500	M5/114.15.2	107636	BioLegend
KLRG1	BV510	1/300	2F1/KLRG1	138421	Biolegend
CD62L	BV570	1/300	MEL-14	104433	Biolegend
CD11b	BV605	1/500	M1/70	101257	Biolegend
CD11c	BV605	1/500	N418	117334	Biolegend
CD19	BV605	1/500	6D5	115540	Biolegend
CD31	BV605	1/300	390	102427	Biolegend
CD4	BV605	1/500	GK1.5	100451	Biolegend
CD8a	BV605	1/500	53-6.7	100744	Biolegend
F4/80	BV605	1/250	BM8	123133	Biolegend
GR1	BV605	1/500	RB6-8C5	108440	BioLegend
ICOS	BV605	1/300	C398.4A	313538	BioLegend
Ki67	BV605	1/750	16A8	652413	BioLegend
TCRb	BV605	1/500	H57-597	109241	Biolegend
TER119	BV605	1/500	TER-119	116239	Biolegend
CD206	BV650	1/300	C068C2	141723	Biolegend
IL-17A	BV650	1/300	TC11-18H10.1	506930	Biolegend
Ly6G	BV650	1/500	1A8	127641	BioLegend
CD19	BV711	1/300	6D5	115555	Biolegend
CD11b	BV750	1/300	M1/70	101267	Biolegend
CD8a	BV785	1/500	53-6.7	100750	Biolegend
CD19	BV785	1/500	6D5	115543	BioLegend
CD44	BV785	1/300	IM7	103059	Biolegend
CD45	BV785	1/300	30-F11	103149	Biolegend
F4/80	BV785	1/250	BM8	123141	Biolegend
IFN-g	BV785	1/250	XMG1.2	505838	Biolegend
NK1.1	BV785	1/500	PK136	108749	Biolegend
NK1.1	BV785	1/500	PK136	108749	BioLegend
Siglec H	FITC	1/250	551	129604	Biolegend
p-STAT3	PE	1/25	13A3-1	651004	BioLegend
Siglec H	PE	1/500	551	129606	Biolegend
CD11b	PECy7	1/500	M1/70	101216	Biolegend
CD4	PECy7	1/500	GK1.5	100422	Biolegend
VCAM1	PECy7	1/300	429 (MVCAM.A)	105720	BioLegend
CD44	PerCP	1/300	IM7	103036	BioLegend
CD44	PerCP Cy5.5	1/300	IM7	103032	Biolegend
SiglecH	PerCP cy5.5	1/250	551	129614	Biolegend
CD11c	PercPCy5.5	1/200	N418	45-0114-82	Thermo Fisher
CD73	PerCPcy5.5	1/300	TY/11.8	127213	Biolegend
CD19	Biotin	1/500	6D5	115504	Biolegend
CD16/32		1/500	2.4G2	CUS-HB-197	Bio X Cell
B220	AF700	1/300	RA3-6B2	56-0452-82	eBioscience
CD11c	AF700	1/500	N418	56-0114-82	ebioscience
CD19	AF700	1/500	eBio1D3 (1D3)	56-0193-82	eBioscience
CD3e	AF700	1/500	eBio500A2	56-0033-82	eBioscience
Gr1	AF700	1/500	RB6-8C5	56-5931-82	eBioscience
TCRb	AF700	1/500	H57-597	56-5961-82	eBioscience
TER-119	AF700	1/500	TER-119	56-5921-82	eBioscience
CCR7	APC	1/200	4B12	17-1971-81	ebioscience
KLRG1	APC	1/500	2F1	17-5893-82	eBioscience
CD8a	Biotin	1/500	53-6.7	13-0081-85	eBioscience
Podoplanin	Biotin	1/500	eBio8.1.1 (8.1.1)	13-5381-82	eBioScience
TCRgd	BV605	1/500	GL3	118129	BioLegend
Arginase -1	EF450	1/300	A1exF5	48-3697-82	eBioscience
CD11c	EF450	1/500	N418	48-0114-82	eBioscience
CD3e	EF450	1/500	145-2C11	48-0031-82	eBioscience
IL-5	PE	1/300	TRFK5	12-7052-82	eBioscience
CD4	PE-Cy5	1/500	GK1.5	15-0041-82	eBioscience
Gata3	PE-Cy5	1/300	TWAJ	15-9966-42	eBioscience
B220	PerCP Cy5.5	1/250	RA3-6B2	45-0452-82	eBioscience
CD19	PECy7	1/500	eBio1D3 (1D3)	25-0193-82	eBioscience
CD3e	PECy7	1/500	145-2C11	25-0031-82	eBioscience
Siglec H	PerCP-efl710	1/250	eBio440c	46-0333-82	eBioscience
ST2	FITC	1/300	DJ8	101001F	mdbio
LIFRa	PE	1/250	673602	FAB59990P	R&D systems
CD11c	AF700	1/500	N418	56-0114-82	Thermo Fisher
CD4	AF700	1/500	GK1.5	56-0041-82	Thermo Fisher
CD45	AF700	1/500	30-F11	56-0451-82	Thermo Fisher

Antibody	Fluorophore	Dilution	Clone	Catalogue number	Supplier
CD317	APC	1/300	eBio927	17-3172-82	Thermo Fisher
ICOS	APC	1/300	C398.4A	17-9949-82	Thermo Fisher
CD19	EF450	1/500	eBio1D3 (1D3)	48-0193-82	Thermo Fisher
Gr1	EF450	1/500	RB6-8C5	48-5931-82	Thermo Fisher
NK1.1	EF450	1/500	PK136	48-5941-82	Thermo Fisher
TCRb	EF450	1/500	H57-597	48-5961-82	Thermo Fisher
Ter119	EF450	1/500	TER-119	48-5921-82	Thermo Fisher
eBioscience Fixable Viability dye	EF780	1/3000		65-0865-18	Thermo Fisher
FcErI	EF450	1/500	MAR-1	48-5898-82	Thermo Fisher
CD62L	FITC	1/300	MEL-14	11-0621-82	Thermo Fisher
CXCR3	FITC	1/500	CXCR3-173	11-1831-82	Thermo Fisher
CD8a	FITC	1/300	53-6.7	11-0081-85	Thermo Fisher
KLRG1	PerCP EF710	1/300	2F1	46-5893-82	Thermo Fisher
Siglec H	PerCP EF710	1/250	eBio440c	46-0333-82	Thermo Fisher
Gata3	PE	1/300	TWAJ	12-9966-42	Thermo Fisher
IL-13	PE	1/300	eBio13A	12-7133-82	Thermo Fisher
KLRG1	PE	1/500	2F1	12-5893-82	Thermo Fisher
CD11c	PECy7	1/500	N418	25-0114-82	Thermo Fisher
CD4	PECy7	1/500	GK1.5	25-0041-82	Thermo Fisher
CD8a	PECy7	1/500	53-6.7	25-0081-82	Thermo Fisher
FcErI	PECy7	1/500	MAR-1	25-5898-82	Thermo Fisher
FoxP3	PECy7	1/300	FJK-16s	25-5773-82	Thermo Fisher
IL-13	PECy7	1/300	eBio13A	25-7133-82	Thermo Fisher
IL-17A	PECy7	1/300	eBio17B7	25-7177-82	Thermo Fisher
Ki67	PECy7	1/500	SolA15	25-5698-82	Thermo Fisher
KLRG1	PECy7	1/500	2F1	25-5893-82	Thermo Fisher
NK1.1	PECy7	1/500	PK136	25-5941-82	Thermo Fisher
CD31	Biotin	1/500	MEC13.3	102504	Biolegend
TCRgd	PECy7	1/500	eBioGL3 (GL-3)	25-5711-82	Thermo Fisher
CD45	PerCP-Cy5.5	1/300	30-F11	45-0451-82	Thermo Fisher
CCR5	PerCP-EF710	1/250	HM-CCR5 (7A4)	46-1951-82	Thermo Fisher

Microscopy

Antibody	Fluorophore	Dilution	Clone	Catalogue number	Supplier
CD3e	PE	1/100	145-2C11	12-0031-82	eBioscience
CD3e	FITC	1/100	145-2C11	11-0031-82	eBioscience
KLRG1	PE	1/100	2F1	12-5893-82	Thermo Fisher
B220	AF700	1/100	RA3-6B2	56-0452-82	eBioscience
CCL21		1/300		AF457	R&D systems
VEGFR3		1/300		BS-2202R	Bioss
Anti-Rat	AF568	1/300		A11077	Thermo Fisher
Anti-Rabbit	AF647	1/300		AB150075	Abcam
Anti-Goat	AF488	1/300		A-11055	Thermo Fisher
Anti LIF		1/300		AB-449-NA	Thermo Fisher
Anti LIF		1/300		AB-449	Thermo Fisher

Protein	Catalogue number	Supplier
Recombinant Mouse LIF	8878-LF	R&D systems
Recombinant Mouse CCL21	457-6C-025	R&D systems
Recombinant Mouse IL-33	580508	Biolegend
Recombinant Mouse FLT3L	550706	Biolegend
Recombinant Mouse IL-7	577808	Biolegend
Recombinant Mouse IL-2	575408	Biolegend
Reagents	**Catalogue number**	**Supplier**
Endothelail grwoth factor	354006	CORNING
FTY720	BML-SL233-0005	Enzo
eBioscience™ Protein Transport Inhibitor Cocktail	00-4980-03	Thermo Fisher
Cell Stimulation Cocktail	00-4970-03	Thermo Fisher
Precision count beads	424902	BioLegend
Ragweed pollen extract		Greer Laboratories
Fluorescein isothiocyanate–dextran	FD40	Sigma-Aldrich
TLR9 Ligand	ODN 2395	Invivogen
BD cytofix/cytoperm		BD Biosciences
eBioscience™ Foxp3 / Transcription Factor Staining Buffer Set	00-5523-00	Thermo Fisher
SuperScript™ IV Reverse Transcriptase	18090010	Thermo Fisher
Oligo(dT)$_{12-18}$ Primer	18418012	Thermo Fisher
TaqMan™ Universal PCR Master Mix	4324018	Thermo Fisher
Power SYBR™ Green PCR Master Mix	4367659	Thermo Fisher
TRIzol™ Reagent	15596026	Thermo Fisher
Direct-zol RNA Microprep Kits	R2061	ZYMO Research
ELISA	**Catalogue number**	**Supplier**
ProcartaPlex Mouse Basic Kit	EPX010-20440-901	Thermo Fisher
LIF Mouse ProcartaPlex™ Simplex Kit	EPX01A-26040-901	Thermo Fisher
IFN-1 Mouse ProcartaPlex™ Simplex Kit	EPX01A-26027-901	Thermo Fisher
IL-5 Mouse ProcartaPlex™ Simplex Kit	EPX01A-20610-901	Thermo Fisher
IgE Mouse Uncoated ELISA Kit	88-50460-88	Thermo Fisher
CCL21 Mouse ProcartaPlex™ Simplex Kit	EPX010-26101-901	Thermo Fisher
CCL19 Mouse ProcartaPlex™ Simplex Kit	EPX010-26069-901	Thermo Fisher
CCL25 Mouse ProcartaPlex™ Simplex Kit	EPX010-26078-901	Thermo Fisher
CXCL9 Mouse ProcartaPlex™ Simplex Kit	EPX010-26061-901	Thermo Fisher
CXCL10 Mouse ProcartaPlex™ Simplex Kit	EPX01A-26018-901	Thermo Fisher

Primers	
PVM FP 5'-GCCTGCATCAACACAGTGTGT	
PVM RP 5'-GCCTGATGTGGCAGTGCTT	
Mouse HPRT FP 5'-AGGCCAGACTTTGTTGGATTTGAA	
Mouse HPRT RP 5'-CAACTTGCGCTCATCTTAGGCTTT	
Hamster GAPDH FP 5'-GACATCAAGAAGGTGGTGAAGCA	
Hamster GAPDH RP 5'-CATCAAAGGTGGAAGAGTGGGA	
Lif gRNA target sequences	
G1 (F) TAATGATTCTAGTTGCCTACAGG	
G2 (F) TGGAGTCCCCATGTCACAGGTGG	
G3 (F) TTCCTCCATCGGTCCAGGAGGGG	
G4 (R) TACCCCTCCTGGACCGATGGAGG	
Screening primers	
P1 TAGGAAGCCAGAGTCTAGTGGCAGTTTTAAGAGATGG	
P2 AAGGCTTCTTTGTCAGAGTGGTCGG	
P2 AAGGCTTCTTTGTCAGAGTGGTCGG	
Primers for generation of probes	
CCTGCCACCCCCTTAACCTCCATAAGTGAAAAGCAAGTGG	
ACTGGGCCTGCTAGGGGTTTGACAG	
TGATGGAGCTGTGGGATGGG	
ACACACTCGGGCTCCATTATGC	
Taqman primers	
CCL21a	Mm03646971_gH
Lif	Mm00434762_g1
Lifr	Mm00442942_m1
Gapdh	Mm99999915_g1

nature portfolio

Corresponding author(s): Andrew McKenzie
Mayuri Gogoi

Last updated by author(s): May 21, 2024

Reporting Summary

Nature Portfolio wishes to improve the reproducibility of the work that we publish. This form provides structure for consistency and transparency in reporting. For further information on Nature Portfolio policies, see our Editorial Policies and the Editorial Policy Checklist.

Statistics

For all statistical analyses, confirm that the following items are present in the figure legend, table legend, main text, or Methods section.

n/a	Confirmed	
☐	☒	The exact sample size (*n*) for each experimental group/condition, given as a discrete number and unit of measurement
☐	☒	A statement on whether measurements were taken from distinct samples or whether the same sample was measured repeatedly
☐	☒	The statistical test(s) used AND whether they are one- or two-sided *Only common tests should be described solely by name; describe more complex techniques in the Methods section.*
☒	☐	A description of all covariates tested
☒	☐	A description of any assumptions or corrections, such as tests of normality and adjustment for multiple comparisons
☐	☒	A full description of the statistical parameters including central tendency (e.g. means) or other basic estimates (e.g. regression coefficient) AND variation (e.g. standard deviation) or associated estimates of uncertainty (e.g. confidence intervals)
☐	☒	For null hypothesis testing, the test statistic (e.g. *F*, *t*, *r*) with confidence intervals, effect sizes, degrees of freedom and *P* value noted *Give P values as exact values whenever suitable.*
☒	☐	For Bayesian analysis, information on the choice of priors and Markov chain Monte Carlo settings
☒	☐	For hierarchical and complex designs, identification of the appropriate level for tests and full reporting of outcomes
☒	☐	Estimates of effect sizes (e.g. Cohen's *d*, Pearson's *r*), indicating how they were calculated

Our web collection on statistics for biologists contains articles on many of the points above.

Software and code

Policy information about availability of computer code

Data collection	BD LSRFortessa Special Order (5 laser), BD BD FACSDiva software V6.2 ID7000 Spectral Cell Analyser (Sony) iCyt Synergy, Sony Biotechnology SY3200 Illumina Hiseq4000 Olympus VS200 slide scanner Luminex MAGPIX
Data analysis	RNA-seq: Sequence data were trimmed to remove adaptors and sequences with a quality score below 30 using Trim Galore (version 0.50, Babraham Bioinformatics) and then aligned to the mouse genome (GRCm38) using STAR (version 2.6.0a), and differential expression was calculated using DESeq2 (version 1.18.1). Prism 9, GraphPad Prism FlowJo. FlowJo, LLC, v10, RRID: SCR_008520 ImageJ2. Verson:2.14.0/1.5f

For manuscripts utilizing custom algorithms or software that are central to the research but not yet described in published literature, software must be made available to editors and reviewers. We strongly encourage code deposition in a community repository (e.g. GitHub). See the Nature Portfolio guidelines for submitting code & software for further information.

Data

Policy information about availability of data

All manuscripts must include a data availability statement. This statement should provide the following information, where applicable:

- Accession codes, unique identifiers, or web links for publicly available datasets
- A description of any restrictions on data availability
- For clinical datasets or third party data, please ensure that the statement adheres to our policy

All high-throughput data in this study were deposited at the Gene Expression Omnibus (GEO) under accession number GSE243691

Research involving human participants, their data, or biological material

Policy information about studies with human participants or human data. See also policy information about sex, gender (identity/presentation), and sexual orientation and race, ethnicity and racism.

Reporting on sex and gender	N/A
Reporting on race, ethnicity, or other socially relevant groupings	N/A
Population characteristics	N/A
Recruitment	N/A
Ethics oversight	N/A

Note that full information on the approval of the study protocol must also be provided in the manuscript.

Field-specific reporting

Please select the one below that is the best fit for your research. If you are not sure, read the appropriate sections before making your selection.

☒ Life sciences ☐ Behavioural & social sciences ☐ Ecological, evolutionary & environmental sciences

For a reference copy of the document with all sections, see nature.com/documents/nr-reporting-summary-flat.pdf

Life sciences study design

All studies must disclose on these points even when the disclosure is negative.

Sample size	Information on sample size is provided within each figure legend. No statistical methods were used to predetermine sample size. Sample size were determined by prior experience as mentioned in the following articles 1 Kerscher, B. et al. BET Bromodomain Inhibitor iBET151 Impedes Human ILC2 Activation and Prevents Experimental Allergic Lung Inflammation. Front Immunol 10, 678 (2019). https://doi.org:10.3389/fimmu.2019.00678 2 Szeto, A. C. H. et al. An alphavbeta3 integrin checkpoint is critical for efficient T(H)2 cell cytokine polarization and potentiation of antigen-specific immunity. Nat Immunol 24, 123-135 (2023). https://doi.org:10.1038/s41590-022-01378-w 3 Panova, V. et al. Group-2 innate lymphoid cell-dependent regulation of tissue neutrophil migration by alternatively activated macrophage-secreted Ear11. Mucosal Immunol 14, 26-37 (2021). https://doi.org:10.1038/s41385-020-0298-2
Data exclusions	No data were excluded from analysis of in vitro experiments. For in vivo experiments, outliers may result from variability in the technical treatment and subsequent suboptimal induction of inflammation. The control groups (PBS/Naive) provide a baseline comparison and are included in our experiments for this purpose. Outliers were identified using the ROUT method in PRISM. Once identified, all parameters from the outlier samples were excluded from analysis.
Replication	All experiments were replicated in at least 2 independent experiments using biologically independent samples (individual mice) within each experiment. All attempts at replication were successful.
Randomization	Sex- and aged- matched control and experimental mice were used in in vivo experiments according to obtained genotypes. Mice were randomly allocated in groups according to their genotypes for both in vivo and in vitro experiments .
Blinding	Investigators were blinded to group allocation during data collection and analysis.

Reporting for specific materials, systems and methods

We require information from authors about some types of materials, experimental systems and methods used in many studies. Here, indicate whether each material, system or method listed is relevant to your study. If you are not sure if a list item applies to your research, read the appropriate section before selecting a response.

Materials & experimental systems

n/a	Involved in the study
☐	☒ Antibodies
☐	☒ Eukaryotic cell lines
☒	☐ Palaeontology and archaeology
☐	☒ Animals and other organisms
☒	☐ Clinical data
☒	☐ Dual use research of concern
☒	☐ Plants

Methods

n/a	Involved in the study
☒	☐ ChIP-seq
☐	☒ Flow cytometry
☒	☐ MRI-based neuroimaging

Antibodies

Antibodies used

Flowcytometry:
Antibody, Fluorophore, Dilution, Clone, Catalogue number, Supplier
CD16/32 1/500 2.4G2 CUS-HB-197 Bio X Cell
CD45 BUV395 1/500 30-F11 565967 BD Biosciences
CD11b BUV395 1/500 M1/70 563553 BD Biosciences
Siglec F AF647 1/500 E50-2440 562680 BD Biosciences
CD4 BUV395 1/500 GK1.5 563790 BD Biosciences
TCRb BUV496 1/250 H57-597 749915 BD Biosciences
CD11b BUV737 1/500 M1/70 612800 BD Biosciences
CD4 BUV737 1/500 RM4-5 612844 BD Biosciences
SA BUV737 BUV737 1/300 612775 BD Biosciences
Thy1.2 (CD90.2) BUV805 1/500 BD 741909 BD Biosciences
CD11b BV750 1/300 M1/70 746910 BD Biosciences
ICAM1 AF647 1/500 YN1/1.7.4 116114 Biolegend
CD19 AF700 1/500 6D5 115528 Biolegend
CD8a AF700 1/500 53-6.7 100730 Biolegend
FcεRIα AF700 1/500 MAR-1 134324 BioLegend
TNF AF700 1/300 MP6-XT22 506338 Biolegend
CD45 APC 0.3 ug in 200 ul 30-F11 17-0451-82 Thermo Fisher
IL5 APC 1/300 TRFK5 504306 BioLegend
CD11b Biotin 1/500 M1/70 101204 Biolegend
CD127 Biotin 1/500 SB/199 121104 Biolegend
CD317 Biotin 1/500 927 127006 Biolegend
CD4 Biotin 1/500 GK1.5 100404 Biolegend
TCRb Biotin 1/500 H57-597 109204 Biolegend
NK1.1 BUV395 1/500 PK136 564144 BD Biosciences
Cd11c BV421 1/500 N418 117330 Biolegend
Gr1 BV421 1/300 RB6-8C5 108433 Biolegend
NK1.1 BV421 1/500 PK136 108731 BioLegend
SA BV421 BV421 1/300 405225 Biolegend
CD25 BV510 1/300 PC61 102042 Biolegend
CD45 BV510 1/500 30-F11 103138 Biolegend
IA/IE BV510 1/500 M5/114.15.2 107636 BioLegend
KLRG1 BV510 1/300 2F1/KLRG1 138421 Biolegend
CD62L BV570 1/300 MEL-14 104433 Biolegend
CD11b BV605 1/500 M1/70 101257 Biolegend
CD11c BV605 1/500 N418 117334 Biolegend
CD19 BV605 1/500 6D5 115540 Biolegend
CD31 BV605 1/300 390 102427 Biolegend
CD4 BV605 1/500 GK1.5 100451 Biolegend
CD8a BV605 1/500 53-6.7 100744 Biolegend
F4/80 BV605 1/250 BM8 123133 Biolegend
GR1 BV605 1/500 RB6-8C5 108440 BioLegend
ICOS BV605 1/300 C398.4A 313538 BioLegend
Ki67 BV605 1/750 16A8 652413 BioLegend
TCRb BV605 1/500 H57-597 109241 Biolegend
TER119 BV605 1/500 TER-119 116239 Biolegend
CD206 BV650 1/300 C068C2 141723 Biolegend
IL-17A BV650 1/300 TC11-18H10.1 506930 Biolegend
Ly6G BV650 1/500 1A8 127641 BioLegend

CD19 BV711 1/300 6D5 115555 Biolegend
CD11b BV750 1/300 M1/70 101267 Biolegend
CD8a BV785 1/500 53-6.7 100750 Biolegend
CD19 BV785 1/500 6D5 115543 BioLegend
CD44 BV785 1/300 IM7 103059 Biolegend
CD45 BV785 1/300 30-F11 103149 Biolegend
F4/80 BV785 1/250 BM8 123141 Biolegend
IFN-g BV785 1/250 XMG1.2 505838 Biolegend
NK1.1 BV785 1/500 PK136 108749 Biolegend
NK1.1 BV785 1/500 PK136 108749 BioLegend
Siglec H FITC 1/250 551 129604 Biolegend
p-STAT3 PE 1/25 13A3-1 651004 BioLegend
Siglec H PE 1/500 551 129606 Biolegend
CD11b PECy7 1/500 M1/70 101216 Biolegend
CD4 PECy7 1/500 GK1.5 100422 Biolegend
VCAM1 PECy7 1/300 429 (MVCAM.A) 105720 BioLegend
CD44 PerCP 1/300 IM7 103036 BioLegend
CD44 PerCP Cy5.5 1/300 IM7 103032 Biolegend
SiglecH PerCP cy5.5 1/250 551 129614 Biolegend
CD11c PercPCy5.5 1/200 N418 45-0114-82 Thermo Fisher
CD73 PerCPcy5.5 1/300 TY/11.8 127213 Biolegend
CD19 Biotin 1/500 6D5 115504 Biolegend
B220 AF700 1/300 RA3-6B2 56-0452-82 eBioscience
CD11c AF700 1/500 N418 56-0114-82 ebioscience
CD19 AF700 1/500 eBio1D3 (1D3) 56-0193-82 eBioscience
CD3e AF700 1/500 eBio500A2 56-0033-82 eBioscience
Gr1 AF700 1/500 RB6-8C5 56-5931-82 eBioscience
TCRb AF700 1/500 H57-597 56-5961-82 eBioscience
TER-119 AF700 1/500 TER-119 56-5921-82 eBioscience
CCR7 APC 1/200 4B12 17-1971-81 ebioscience
KLRG1 APC 1/500 2F1 17-5893-82 eBioscience
CD8a Biotin 1/500 53-6.7 13-0081-85 eBioscience
Podoplanin Biotin 1/500 eBio8.1.1 (8.1.1) 13-5381-82 eBioScience
TCRgd BV605 1/500 GL3 118129 BioLegend
Arginase -1 EF450 1/300 A1exF5 48-3697-82 eBioscience
CD11c EF450 1/500 N418 48-0114-82 eBioscience
CD3e EF450 1/500 145-2C11 48-0031-82 eBioscience
IL-5 PE 1/300 TRFK5 12-7052-82 eBioscience
CD4 PE-Cy5 1/500 GK1.5 15-0041-82 eBioscience
Gata3 PE-Cy5 1/300 TWAJ 15-9966-42 eBioscience
B220 PerCP Cy5.5 1/250 RA3-6B2 45-0452-82 eBioscience
CD19 PECy7 1/500 eBio1D3 (1D3) 25-0193-82 eBioscience
CD3e PECy7 1/500 145-2C11 25-0031-82 eBioscience
Siglec H PerCP-efl710 1/250 eBio440c 46-0333-82 eBioscience
ST2 FITC 1/300 DJ8 101001F mdbio
LIFRa PE 1/250 673602 FAB59990P R&D systems
CD11c AF700 1/500 N418 56-0114-82 Thermo Fisher
CD4 AF700 1/500 GK1.5 56-0041-82 Thermo Fisher
CD45 AF700 1/500 30-F11 56-0451-82 Thermo Fisher
CD317 APC 1/300 eBio927 17-3172-82 Thermo Fisher
ICOS APC 1/300 C398.4A 17-9949-82 Thermo Fisher
CD19 EF450 1/500 eBio1D3 (1D3) 48-0193-82 Thermo Fisher
Gr1 EF450 1/500 RB6-8C5 48-5931-82 Thermo Fisher
NK1.1 EF450 1/500 PK136 48-5941-82 Thermo Fisher
TCRb EF450 1/500 H57-597 48-5961-82 Thermo Fisher
Ter119 EF450 1/500 TER-119 48-5921-82 Thermo Fisher
eBioscience Fixable Viability dye EF780 1/3000 65-0865-18 Thermo Fisher
FcErI EF450 1/500 MAR-1 48-5898-82 Thermo Fisher
CD62L FITC 1/300 MEL-14 11-0621-82 Thermo Fisher
CXCR3 FITC 1/500 CXCR3-173 11-1831-82 Thermo Fisher
CD8a FITC 1/300 53-6.7 11-0081-85 Thermo Fisher
KLRG1 PerCP EF710 1/300 2F1 46-5893-82 Thermo Fisher
Siglec H PerCP EF710 1/250 eBio440c 46-0333-82 Thermo Fisher
Gata3 PE 1/300 TWAJ 12-9966-42 Thermo Fisher
IL-13 PE 1/300 eBio13A 12-7133-82 Thermo Fisher
KLRG1 PE 1/500 2F1 12-5893-82 Thermo Fisher
CD11c PECy7 1/500 N418 25-0114-82 Thermo Fisher
CD4 PECy7 1/500 GK1.5 25-0041-82 Thermo Fisher
CD8a PECy7 1/500 53-6.7 25-0081-82 Thermo Fisher
FcErI PECy7 1/500 MAR-1 25-5898-82 Thermo Fisher
FoxP3 PECy7 1/300 FJK-16s 25-5773-82 Thermo Fisher
IL-13 PECy7 1/300 eBio13A 25-7133-82 Thermo Fisher
IL-17A PECy7 1/300 eBio17B7 25-7177-82 Thermo Fisher
Ki67 PECy7 1/500 SolA15 25-5698-82 Thermo Fisher
KLRG1 PECy7 1/500 2F1 25-5893-82 Thermo Fisher
NK1.1 PECy7 1/500 PK136 25-5941-82 Thermo Fisher

CD31 Biotin 1/500 MEC13.3 102504 Biolegend
TCRgd PECy7 1/500 eBioGL3 (GL-3) 25-5711-82 Thermo Fisher
CD45 PerCP-Cy5.5 1/300 30-F11 45-0451-82 Thermo Fisher
CCR5 PerCP-EF710 1/250 HM-CCR5 (7A4) 46-1951-82 Thermo Fisher

Microscopy
Antibody Fluorophore Dilution Clone Catalogue number Supplier
CD3e PE 1/100 145-2C11 12-0031-82 eBioscience
CD3e FITC 1/100 145-2C11 11-0031-82 eBioscience
KLRG1 PE 1/100 2F1 12-5893-82 Thermo Fisher
B220 AF700 1/100 RA3-6B2 56-0452-82 eBioscience
VEGFR3 1/300 BS-2202R Bioss
Anti-Rat AF568 1/300 A11077 Thermo Fisher
Anti-Rabbit AF647 1/300 AB150075 Abcam
Anti-Goat AF488 1/300 A-11055 Thermo Fisher

Validation

All used ELISA kits and antibodies are commercially available and have been validated by the manufacturer. Validations and detail product information are available on thewebsites:
Flowcytometry:
https://bioxcell.com/recombimab-anti-mouse-cd16-cd32-cp025
https://www.bdbiosciences.com/en-ca/products/reagents/flow-cytometry-reagents/research-reagents/single-color-antibodies-ruo/buv395-rat-anti-mouse-cd45.565967
https://www.bdbiosciences.com/en-ca/products/reagents/flow-cytometry-reagents/research-reagents/single-color-antibodies-ruo/buv395-rat-anti-cd11b.565976
https://www.bdbiosciences.com/en-ca/products/reagents/flow-cytometry-reagents/research-reagents/single-color-antibodies-ruo/alexa-fluor-647-rat-anti-mouse-siglec-f.562680
https://www.bdbiosciences.com/en-ca/products/reagents/flow-cytometry-reagents/research-reagents/single-color-antibodies-ruo/buv395-rat-anti-mouse-cd4.563790
https://www.bdbiosciences.com/en-ca/products/reagents/flow-cytometry-reagents/research-reagents/single-color-antibodies-ruo/buv496-hamster-anti-mouse-tcr-chain.749915
https://www.bdbiosciences.com/en-ca/products/reagents/flow-cytometry-reagents/research-reagents/single-color-antibodies-ruo/buv737-rat-anti-cd11b.741722
https://www.bdbiosciences.com/en-ca/products/reagents/flow-cytometry-reagents/research-reagents/single-color-antibodies-ruo/buv737-rat-anti-mouse-cd4.612844
https://www.bdbiosciences.com/en-ca/products/reagents/flow-cytometry-reagents/research-reagents/single-color-antibodies-ruo/buv737-streptavidin.612775
https://www.bdbiosciences.com/en-ca/products/reagents/flow-cytometry-reagents/research-reagents/single-color-antibodies-ruo/buv805-rat-anti-mouse-cd90-2.741909
https://www.bdbiosciences.com/en-ca/products/reagents/flow-cytometry-reagents/research-reagents/single-color-antibodies-ruo/bv750-rat-anti-cd11b.746910
https://www.biolegend.com/en-gb/products/alexa-fluor-647-anti-mouse-cd54-antibody-3110
https://www.biolegend.com/en-gb/products/alexa-fluor-700-anti-mouse-cd19-antibody-3391
https://www.biolegend.com/en-gb/products/alexa-fluor-700-anti-mouse-cd8a-antibody-3387
https://www.biolegend.com/en-gb/products/alexa-fluor-700-anti-mouse-fcepsilonrialpha-antibody-12817
https://www.biolegend.com/en-gb/products/alexa-fluor-700-anti-mouse-tnf-alpha-antibody-9146
https://www.thermofisher.com/antibody/product/CD45-Antibody-clone-30-F11-Monoclonal/17-0451-82
https://www.biolegend.com/en-gb/products/apc-anti-mouse-human-il-5-antibody-989
https://www.biolegend.com/en-gb/products/biotin-anti-mouse-human-cd11b-antibody-346
https://www.biolegend.com/en-gb/products/biotin-anti-mouse-cd127-il-7ralpha-antibody-3048

https://www.biolegend.com/en-gb/products/biotin-anti-mouse-cd317-bst2-pdca-1-antibody-6348
https://www.biolegend.com/en-gb/products/biotin-anti-mouse-cd4-antibody-247
https://www.biolegend.com/en-gb/products/biotin-anti-mouse-tcr-beta-chain-antibody-269
https://www.bdbiosciences.com/en-ca/products/reagents/flow-cytometry-reagents/research-reagents/single-color-antibodies-ruo/buv395-mouse-anti-mouse-nk-1-1.564144
https://www.biolegend.com/en-gb/products/brilliant-violet-421-anti-mouse-cd11c-antibody-7149
https://www.biolegend.com/en-gb/products/brilliant-violet-421-anti-mouse-ly-6g-ly-6c-gr-1-antibody-7201
https://www.biolegend.com/en-gb/products/brilliant-violet-421-anti-mouse-nk-1-1-antibody-7150
https://www.biolegend.com/en-gb/products/brilliant-violet-421-streptavidin-7297
https://www.biolegend.com/en-gb/products/brilliant-violet-510-anti-mouse-cd25-antibody-8663
https://www.biolegend.com/en-gb/products/brilliant-violet-510-anti-mouse-cd45-antibody-7995
https://www.biolegend.com/en-gb/products/brilliant-violet-510-anti-mouse-i-a-i-e-antibody-7997
https://www.biolegend.com/en-gb/products/brilliant-violet-510-anti-mouse-human-klrg1-mafa-antibody-9943
https://www.biolegend.com/en-gb/products/brilliant-violet-570-anti-mouse-cd62l-antibody-7369
https://www.biolegend.com/en-gb/products/brilliant-violet-605-anti-mouse-human-cd11b-antibody-7637
https://www.biolegend.com/en-gb/products/brilliant-violet-605-anti-mouse-cd11c-antibody-7865
https://www.biolegend.com/en-gb/products/brilliant-violet-605-anti-mouse-cd19-antibody-7645
https://www.biolegend.com/en-gb/products/brilliant-violet-605-anti-mouse-cd31-antibody-9963
https://www.biolegend.com/en-gb/products/brilliant-violet-605-anti-mouse-cd4-antibody-10708
https://www.biolegend.com/en-gb/products/brilliant-violet-605-anti-mouse-cd8a-antibody-7636
https://www.biolegend.com/en-gb/products/brilliant-violet-605-anti-mouse-f4-80-antibody-8702
https://www.biolegend.com/en-gb/products/brilliant-violet-605-anti-mouse-ly-6g-ly-6c-gr-1-antibody-8724
https://www.biolegend.com/en-gb/products/brilliant-violet-605-anti-human-mouse-rat-cd278-icos-antibody-14371
https://www.biolegend.com/en-us/products/brilliant-violet-605-anti-mouse-tcr-beta-chain-antibody-13533

https://www.biolegend.com/en-us/products/brilliant-violet-605-anti-mouse-ter-119-erythroid-cells-antibody-8839
https://www.biolegend.com/en-us/products/brilliant-violet-650-anti-mouse-cd206-mmr-antibody-8842
https://www.biolegend.com/en-us/products/brilliant-violet-650-anti-mouse-il-17a-antibody-7684
https://www.biolegend.com/en-us/products/brilliant-violet-650-anti-mouse-ly-6g-antibody-11981
https://www.biolegend.com/en-us/products/brilliant-violet-711-anti-mouse-cd19-antibody-12075
https://www.biolegend.com/en-us/products/brilliant-violet-750-anti-mousehuman-cd11b-antibody-17501
https://www.biolegend.com/en-us/products/brilliant-violet-785-anti-mouse-cd8a-antibody-7957
https://www.biolegend.com/en-us/products/brilliant-violet-785-anti-mouse-cd19-antibody-7962
https://www.biolegend.com/en-us/products/brilliant-violet-785-anti-mouse-cd19-antibody-7962
https://www.biolegend.com/en-us/products/brilliant-violet-785-anti-mouse-human-cd44-antibody-7959
https://www.biolegend.com/en-us/products/brilliant-violet-785-anti-mouse-cd45-antibody-10636
https://www.biolegend.com/en-us/products/brilliant-violet-785-anti-mouse-f4-80-antibody-9919
https://www.biolegend.com/en-us/products/brilliant-violet-785-anti-mouse-ifn-gamma-antibody-7987
https://www.biolegend.com/en-us/products/brilliant-violet-785-anti-mouse-nk-1-1-antibody-10367
https://www.biolegend.com/en-us/products/brilliant-violet-785-anti-mouse-nk-1-1-antibody-10367
https://www.biolegend.com/en-us/products/fitc-anti-mouse-siglec-h-antibody-5177
https://www.biolegend.com/en-us/products/pe-anti-stat3-phospho-tyr705-antibody-12914
https://www.biolegend.com/en-us/products/pe-anti-mouse-siglec-h-antibody-5178
https://www.biolegend.com/en-us/products/pe-cyanine7-anti-mouse-human-cd11b-antibody-1921
https://www.biolegend.com/en-us/products/pe-cyanine7-anti-mouse-cd4-antibody-1919
https://www.biolegend.com/en-us/products/pe-cyanine7-anti-mouse-cd106-antibody-6135
https://www.biolegend.com/en-us/products/percp-anti-mouse-human-cd44-antibody-6895
https://www.biolegend.com/en-us/products/percp-cyanine5-5-anti-mouse-human-cd44-antibody-5605
https://www.biolegend.com/en-us/products/percp-cyanine5-5-anti-mouse-siglec-h-antibody-6927
https://www.thermofisher.com/antibody/product/CD11c-Antibody-clone-N418-Monoclonal/45-0114-82
https://www.biolegend.com/en-us/products/percp-cyanine5-5-anti-mouse-cd73-antibody-7895
https://www.biolegend.com/en-us/products/biotin-anti-mouse-cd19-antibody-1527
https://www.thermofisher.com/antibody/product/CD45R-B220-Antibody-clone-RA3-6B2-Monoclonal/56-0452-82
https://www.thermofisher.com/antibody/product/CD11c-Antibody-clone-118-A5-Monoclonal/14-9761-82
https://www.thermofisher.com/antibody/product/CD11c-Antibody-clone-N418-Monoclonal/56-0114-82
https://www.thermofisher.com/antibody/product/CD19-Antibody-clone-eBio1D3-1D3-Monoclonal/56-0193-82
https://www.thermofisher.com/antibody/product/Ly-6G-Ly-6C-Antibody-clone-RB6-8C5-Monoclonal/56-5931-82
https://www.thermofisher.com/antibody/product/TCR-beta-Antibody-clone-H57-597-Monoclonal/56-5961-82
https://www.thermofisher.com/antibody/product/TER-119-Antibody-clone-TER-119-Monoclonal/56-5921-82
https://www.thermofisher.com/antibody/product/CD197-CCR7-Antibody-clone-4B12-Monoclonal/17-1971-82
https://www.thermofisher.com/antibody/product/KLRG1-Antibody-clone-2F1-Monoclonal/17-5893-82
https://www.thermofisher.com/antibody/product/CD8a-Antibody-clone-53-6-7-Monoclonal/13-0081-82
https://www.thermofisher.com/antibody/product/Podoplanin-Antibody-clone-eBio8-1-1-8-1-1-Monoclonal/13-5381-82
https://www.biolegend.com/en-gb/products/brilliant-violet-605-anti-mouse-tcr-gamma-delta-antibody-9655?GroupID=BLG3687
https://www.thermofisher.com/antibody/product/Arginase-1-Antibody-clone-A1exF5-Monoclonal/48-3697-82
https://www.thermofisher.com/antibody/product/CD11c-Antibody-clone-N418-Monoclonal/48-0114-82
https://www.thermofisher.com/antibody/product/CD3e-Antibody-clone-145-2C11-Monoclonal/48-0031-82
https://www.thermofisher.com/antibody/product/IL-5-Antibody-clone-TRFK5-Monoclonal/12-7052-82
https://www.thermofisher.com/antibody/product/CD4-Antibody-clone-GK1-5-Monoclonal/15-0041-82
https://www.thermofisher.com/antibody/product/Gata-3-Antibody-clone-TWAJ-Monoclonal/15-9966-42
https://www.thermofisher.com/antibody/product/CD45R-B220-Antibody-clone-RA3-6B2-Monoclonal/14-0452-82

https://www.thermofisher.com/antibody/product/CD19-Antibody-clone-eBio1D3-1D3-Monoclonal/25-0193-82
https://rnaidesigner.thermofisher.com/antibody/product/CD3e-Antibody-clone-145-2C11-Monoclonal/25-0031-82
https://rnaidesigner.thermofisher.com/antibody/product/SIGLEC-H-Antibody-clone-eBio440c-Monoclonal/46-0333-82
https://www.mdbioproducts.com/products/t1-st2-il-33-r-mouse-monoclonal-antibody?variant=39848199422141
https://www.rndsystems.com/products/mouse-lifralpha-pe-conjugated-antibody-673602_fab5990p
https://www.thermofisher.com/antibody/product/CD11c-Antibody-clone-N418-Monoclonal/56-0114-82
https://www.thermofisher.com/antibody/product/CD4-Antibody-clone-GK1-5-Monoclonal/56-0041-82
https://www.thermofisher.com/antibody/product/CD45-Antibody-clone-30-F11-Monoclonal/56-0451-82
https://tfcom-global-nginx.commerceprod.thermofisher.com/antibody/product/CD317-BST2-PDCA-1-Antibody-clone-eBio927-Monoclonal/17-3172-82
https://www.thermofisher.com/antibody/product/CD278-ICOS-Antibody-clone-C398-4A-Monoclonal/17-9949-82
https://www.thermofisher.com/antibody/product/CD19-Antibody-clone-eBio1D3-1D3-Monoclonal/48-0193-82
https://www.thermofisher.com/antibody/product/Ly-6G-Ly-6C-Antibody-clone-RB6-8C5-Monoclonal/48-5931-82
https://www.thermofisher.com/antibody/product/NK1-1-Antibody-clone-PK136-Monoclonal/48-5941-82
https://www.thermofisher.com/antibody/product/TCR-beta-Antibody-clone-H57-597-Monoclonal/48-5961-82
https://www.thermofisher.com/antibody/product/TER-119-Antibody-clone-TER-119-Monoclonal/48-5921-82
https://www.thermofisher.com/order/catalog/product/65-0865-18
https://www.thermofisher.com/antibody/product/FceR1-alpha-Antibody-clone-MAR-1-Monoclonal/48-5898-82
https://www.thermofisher.com/antibody/product/CD62L-L-Selectin-Antibody-clone-MEL-14-Monoclonal/11-0621-82
https://www.thermofisher.com/antibody/product/CD183-CXCR3-Antibody-clone-CXCR3-173-Monoclonal/11-1831-82
https://www.thermofisher.com/antibody/product/CD8a-Antibody-clone-53-6-7-Monoclonal/11-0081-82
https://www.thermofisher.com/antibody/product/KLRG1-Antibody-clone-2F1-Monoclonal/46-5893-82
https://rnaidesigner.thermofisher.com/antibody/product/SIGLEC-H-Antibody-clone-eBio440c-Monoclonal/46-0333-82
https://www.thermofisher.com/antibody/product/Gata-3-Antibody-clone-TWAJ-Monoclonal/12-9966-42
https://www.thermofisher.com/antibody/product/IL-13-Antibody-clone-eBio13A-Monoclonal/12-7133-82
https://rnaidesigner.thermofisher.com/antibody/product/KLRG1-Antibody-clone-2F1-Monoclonal/12-5893-82

https://www.thermofisher.com/antibody/product/CD11c-Antibody-clone-N418-Monoclonal/25-0114-82
https://www.thermofisher.com/antibody/product/CD4-Antibody-clone-GK1-5-Monoclonal/25-0041-82
https://www.thermofisher.com/antibody/product/CD8a-Antibody-clone-53-6-7-Monoclonal/25-0081-82
https://www.thermofisher.com/antibody/product/FceR1-alpha-Antibody-clone-MAR-1-Monoclonal/25-5898-82
https://www.thermofisher.com/antibody/product/FOXP3-Antibody-clone-FJK-16s-Monoclonal/25-5773-82
https://www.thermofisher.com/antibody/product/IL-13-Antibody-clone-eBio13A-Monoclonal/25-7133-82
https://www.thermofisher.com/antibody/product/IL-17A-Antibody-clone-eBio17B7-Monoclonal/25-7177-82
https://www.thermofisher.com/antibody/product/Ki-67-Antibody-clone-SolA15-Monoclonal/25-5698-82
https://www.thermofisher.com/antibody/product/KLRG1-Antibody-clone-2F1-Monoclonal/25-5893-82
https://www.thermofisher.com/antibody/product/NK1-1-Antibody-clone-PK136-Monoclonal/25-5941-82
https://www.biolegend.com/en-gb/search-results/biotin-anti-mouse-cd31-antibody-376
https://www.thermofisher.com/antibody/product/TCR-gamma-delta-Antibody-clone-eBioGL3-GL-3-GL3-Monoclonal/25-5711-82
https://www.thermofisher.com/antibody/product/CD45-Antibody-clone-30-F11-Monoclonal/45-0451-82
https://rnaidesigner.thermofisher.com/antibody/product/CD195-CCR5-Antibody-clone-HM-CCR5-7A4-Monoclonal/46-1951-82

Microscopy
https://www.thermofisher.com/antibody/product/CD3e-Antibody-clone-145-2C11-Monoclonal/12-0031-82
https://www.thermofisher.com/antibody/product/CD3e-Antibody-clone-145-2C11-Monoclonal/11-0031-82
https://rnaidesigner.thermofisher.com/antibody/product/KLRG1-Antibody-clone-2F1-Monoclonal/12-5893-82
https://www.thermofisher.com/antibody/product/CD45R-B220-Antibody-clone-RA3-6B2-Monoclonal/56-0452-82
https://www.biossantibodies.com/datasheets/bs-2202R
https://www.thermofisher.com/antibody/product/Goat-anti-Rat-IgG-H-L-Cross-Adsorbed-Secondary-Antibody-Polyclonal/A-11077
https://www.abcam.com/products/secondary-antibodies/donkey-rabbit-igg-hl-alexa-fluor-647-ab150075.html
https://www.thermofisher.com/antibody/product/Donkey-anti-Goat-IgG-H-L-Cross-Adsorbed-Secondary-Antibody-Polyclonal/A-11055

Eukaryotic cell lines

Policy information about cell lines and Sex and Gender in Research

Cell line source(s)	BHK-21 clone 13 cell line (immortalized cell line derived from hamster kidney) RRID:CVCL_1915
Authentication	Cell lines were not authenticated but were uitiized within 10 passages of a master stock
Mycoplasma contamination	Not tested
Commonly misidentified lines (See ICLAC register)	This cell line isn't listed on the ICLAC database

Animals and other research organisms

Policy information about studies involving animals; ARRIVE guidelines recommended for reporting animal research, and Sex and Gender in Research

Laboratory animals	C57BL/6JOla controls were bred in MRC-LMB. All mice were either on the C57BL/6J Ola background or back-crossed for at least six generations. Il7raCre (Schlenner, S. M. et al. Fate mapping reveals separate origins of T cells and myeloid lineages in the thymus. Immunity 32, 426-436 (2010)) Roraflox/flox (Oliphant, C. J. et al. MHCII-mediated dialog between group 2 innate lymphoid cells and CD4(+) T cells potentiates type 2 immunity and promotes parasitic helminth expulsion. Immunity 41, 283-295 (2014)) Il1rl1−/− (Townsend, M. J., Fallon, P. G., Matthews, D. J., Jolin, H. E. & McKenzie, A. N. T1/ST2-deficient mice demonstrate the importance of T1/ST2 in developing primary T helper cell type 2 responses. J Exp Med 191, 1069-1076 (2000)) Rag2−/− Rag2−/−Il2rgc−/− (Rag2−/−gc−/−) Lif flox/flox,MRC-LMB, accompanying manuscript BIC mice (Il13Dre, Cd28Vika, IcosCre), (Szeto, Clarke et al., Science, in press) ILC2LIFKO mice were BIC Lif flox/flox mice MRC-LMB, accompanying manuscript SiglechCre, Puttur, F. et al. Absence of Siglec-H in MCMV infection elevates interferon alpha production but does not enhance viral clearance. PLoS Pathog 9, e1003648 (2013) Lifr−/flox, MGI:4841519 All mice were maintained in the Medical Research Council ARES animal facility under specific pathogen-free conditions, at 19-23°C, 45-65% humidity, with a 12-h light-dark cycle. Mice used in the experiments were between 8-16 weeks old. In individual experiments, mice were matched for age, sex and background strain.
Wild animals	The study did not involve wild animals.
Reporting on sex	Mice were sex matched for in vivo experiments (within one experiment, n=3-10 per group) and both male and female cohorts (2-3

Reporting on sex	independent experiments) were used in this study , for each reported findings. For in vitro experiments male and female mice were used.
Field-collected samples	The study did not involve samples collected from the field.
Ethics oversight	All experiments undertaken in this study were done so with the approval of the LMB Animal Welfare and Ethical Review Body (AWERB) and of the UK Home Office.

Note that full information on the approval of the study protocol must also be provided in the manuscript.

Plants

Seed stocks	*Report on the source of all seed stocks or other plant material used. If applicable, state the seed stock centre and catalogue number. If plant specimens were collected from the field, describe the collection location, date and sampling procedures.*
Novel plant genotypes	*Describe the methods by which all novel plant genotypes were produced. This includes those generated by transgenic approaches, gene editing, chemical/radiation-based mutagenesis and hybridization. For transgenic lines, describe the transformation method, the number of independent lines analyzed and the generation upon which experiments were performed. For gene-edited lines, describe the editor used, the endogenous sequence targeted for editing, the targeting guide RNA sequence (if applicable) and how the editor was applied.*
Authentication	*Describe any authentication procedures for each seed stock used or novel genotype generated. Describe any experiments used to assess the effect of a mutation and, where applicable, how potential secondary effects (e.g. second site T-DNA insertions, mosiacism, off-target gene editing) were examined.*

Flow Cytometry

Plots

Confirm that:

☒ The axis labels state the marker and fluorochrome used (e.g. CD4-FITC).

☒ The axis scales are clearly visible. Include numbers along axes only for bottom left plot of group (a 'group' is an analysis of identical markers).

☒ All plots are contour plots with outliers or pseudocolor plots.

☒ A numerical value for number of cells or percentage (with statistics) is provided.

Methodology

Sample preparation	Tissue preparation. Lung tissue was predigested with 750 U ml-1 collagenase I (Gibco) and 0.3 mg ml-1 DNaseI (Sigma-Aldrich) before obtaining a single-cell suspension at 37 °C for 30 min; the tissue was passed through a 70 µm cell strainer. For lymphocyte enrichment, lung single-cell suspension was centrifuged through 30% Percoll (GE Healthcare) at 800 x g for 15 min. Spleen, thymus and mediastinal lymph node single cell suspensions were prepared by passing the tissue through a 70 µM cell strainer and lysing RBCs. Single bone marrow cell suspensions were prepared by flushing the femur and tibia with endotoxin-free PBS and lysing RBCs.
Instrument	ID7000 spectral cell analyser (Sony) LSRFortessa system (BD Biosciences) for analysis, iCyt Synergy system (70-um nozzle, Sony Biotechnology) for cell sorting.
Software	FACSDiva sofware (version 6.2, BD Biosciences) FlowJo. FlowJo, LLC, v10, RRID: SCR_008520
Cell population abundance	Purity of sorted populations is typically >97%, as determined by analysis of sorted cells by flow cytometry.
Gating strategy	Cells are defined in FSC/SCC plot, followed by doublet exclusion in FCS-A/FCS-H plot. Positive populations are defined by comparison to unstained controls, isotype controls or fluorescence minus one controls.

☒ Tick this box to confirm that a figure exemplifying the gating strategy is provided in the Supplementary Information.